Circuits and Antennas Incorporating Gallium-based Liquid Metal

Yi-Wen Wu, *Member, IEEE,* Shaker Alkaraki, *Member, IEEE,* Shiyang Tang, Yi Wang, *Senior Member, IEEE,* James Kelly, *Member, IEEE*

***Abstract*— This paper reviews the application and technology advancement of Gallium (Ga)-based liquid metal (LM) in high-frequency circuits and antennas. It discusses the material properties of common liquid metals, the fluidic channels used to contain LM and their manufacturing techniques, and the actuation techniques, which are all critical for the design and implementation of LM-based devices. LM's fluidic and pliable nature, together with its excellent electrical, thermal, and rheological (i.e. fluid flow) properties, provides some unique and innovative solutions to flexible/wearable electronics, reconfigurable circuits and antennas. The paper provides a comprehensive review of a wide range of LM-enabled high-frequency circuits and antennas, including: interconnects and transitions, reconfigurable passive circuits (such as resonators, filters, and couplers), switches, phase shifters, reconfigurable antennas, flexible and wearable antennas, and metamaterials (i.e. periodic materials with properties not found in nature). The paper presents various design concepts and implementation techniques, highlights key capabilities, discusses the challenges and opportunities with the use of Ga-based liquid metal materials.**

***Index Terms*— Antennas, liquid metal, microfluidic channels, reconfigurable circuits.**

I. Introduction

The term liquid metal (LM) refers to metals that are liquid at room temperature [1]-[10]. Liquid metals have the unique attribute of being highly conductive while remaining fluidic and pliable. These properties endow them with a wide range of applications in microfluidics, biomedical and wearable devices, and flexible electronics [1, 2, 4, 5, 8]. Mercury is the best known and earliest explored liquid metal material in electronics. However, its toxicity has prevented its wide usage. The widespread interest in liquid metals has only been reignited when the benign Gallium (Ga)-based liquid metals and alloys came into view of the electronic community in around 2007 [11]. Liquid metals have been used in flexible devices, wearable sensors, and more recently in high-frequency circuits and antennas – the subject of this review. They have also been used for thermal managements in electronics.

There have been several surveys and reviews on liquid metals focusing on actuation techniques [12]-[34], biomedical and wearable applications [35], or flexible electronics [36]-[38]. However, there is not yet a comprehensive review dedicated to microwave frequency circuits and antennas as this has become a major application area for liquid metals. The only review published in IEEE was Sen and Kim's review on microscale liquid-metal switches [39] in 2009. A lot of the work surveyed then was based on mercury.

This paper reviews the use of Ga-based liquid metals in high-frequency circuits and antennas. We will examine a range of topics from the material properties of the liquid metals (Section II), four main actuation methods (Section III), the manufacturing techniques related to microfluidic channels (Section IV), to the applications in a variety of circuits and antennas. These include interconnects and transition structures (Section V), reconfigurable circuits (such as resonators, filters and couplers in Section VI), switches (Section VII), phase shifters (Section VIII), frequency/pattern/polarization-reconfigurable antennas (Section IX), metamaterials (Section X), and flexible/stretchable/wearable antennas (Section XI). Finally, Section XII draws conclusions.

II. Electrical, Thermal, and Mechanical Properties

According to the periodic table, the following metals are liquid at or near room temperature: Mercury (Hg), Cesium (Cs), Rubidium (Rb), and Gallium (Ga) [1]. Hg has a melting point of -38.8°C, can evaporate at room temperature and is highly toxic [1]-[3]. Cs and Rb are easily oxidized in air and react violently with water. These properties are not conducive to the stable operation of electronic equipment. Ga is an important raw material for semiconductors, and its melting point is 29.8°C [1]. A eutectic is a mixture of substances that melts at a single temperature that is lower than the melting points of the separate constituents. Eutectic alloys of Ga with other post-transition metals such as Indium (In), Tin (Sn), and Lead (Pb) offer properties such as low melting temperatures or high electrical conductivity, making them attractive for various applications [1]-[9]. Among them, eutectic Ga-In-Sn alloy (Galinstan; 68.5wt% Ga, 21.5wt% In and 10wt% Sn) and eutectic Ga-In alloy (EGaIn; 75.5wt% Ga and 24.5wt% In) are two commercially available LM alloys [4]. Table I compares the

This work was supported by UK Engineering and Physical Sciences Research Council grants EP/V008382/1 and EP/V008420/1.

Y. Wu, S. Tang, and Y. Wang are with School of Engineering, University of Birmingham, B15 2TT, United Kingdom (e-mail: {y.wu.7, s.tang, y.wang.1}@bham.ac.uk).

S. Alkaraki and J. Kelly are with the School of Electronic Engineering and Computer Science, Queen Mary University of London, London (email: {s.m.alkaraki, j.kelly}@qmul.ac.uk).

TABLE I

COMPARISON OF COMMON LIQUID METALS

Property	Hg	Ga	$Ga^{68.5}In^{21.5}Sn^{10}$ (Galinstan)	$Ga^{67}In^{20.5}Sn^{12.5}$	$Ga^{75.5}In^{24.5}$ (EGaIn)	Water
Melting point (°C)**	-38.8 [2, 3, 4]	29.8 [2, 3, 4]	11* [8]	10.5 [2]	15.5 [2,4]	0 [3, 4]
Boiling point (°C)	356 [2, 3, 4]	2205 [2, 3, 4]	>1300 [4, 6, 7]	>1300 [2]	2000 [2, 4]	100 [3, 4]
Electrical Conductivity (S/m)	1.04×10^6 [2, 4]	6.73×10^6 [4]	3.46×10^6 [4]	3.1×10^6 [2]	3.4×10^6 [2,4]	$<5\times10^{-4}$ [4]
Thermal Conductivity (W/(m·K))	8.5 [4]	29.3 [4]	16.5 [4, 6, 7]	N.A.	26.6 [4]	0.6 [3, 4]
Viscosity (Pa·s)	1.53×10^{-3} [4]	1.37×10^{-3} [4]	2.4×10^{-3} [4, 6, 7]	N.A.	1.99×10^{-3} [4]	1×10^{-3} [4]
Surface Tension (N/m)	0.487 [4]	0.707 [2, 4]	0.718 [4]	0.533 [2]	0.624 [2,4]	0.072 [4]
Density (kg/m^3)	1353 [2, 3, 4]	6093 [2, 3, 4]	6440 [4, 6]	6360 [2]	6280 [2,4]	998 [3, 4]
Vapor pressure (Pa)	1@ 42 ºC [4]	$\sim10^{-35}$ @ 29.9 ºC [4]	$<1.33\times10^{-6}$ @ 500 ºC [4, 6]	N.A.	N.A.	3169 @ 25 ºC [4]
Toxicity	Toxic [4, 5]	Low toxicity [4, 5]	Low toxicity [4, 5, 6, 10]	Low toxicity [4, 5, 6]	Low toxicity [4, 5, 6]	Nontoxic

Note: * Galinstan's melting point is usually reported as -19ºC. It refers to the freezing temperature, which may result from the proclivity of liquid metals to supercool [1, 8]. **The melting point of other post transition metals or eutectic alloys: In (156.6°C), Sn (231.9°C), Pb (327.5°C), $Ga^{91.7}Sn^{8.3}$ (21°C), $Ga^{4.7}Pb^{95.3}$ (317°C), and so on [1].

properties of various LMs [1]-[10]. LMs based on alloys of Ga have several important advantages, including low melting points, low toxicity, relatively low chemical reactivity due to the formation of a self-limiting oxide skin, low viscosity, high surface tension, superior electrical and thermal conductivities compared with Hg, and excellent wettability to various substrates.

When Ga-based alloys are exposed to air, an oxide layer forms on the surface, which prevents further oxidation [1, 4, 5, 9]. Ga-based alloys have a viscosity around twice that of water, indicating good fluidity [1]-[4]. The electrical conductivities of Galinstan and EGaIn alloys are 3.8×10^6 S/m and 3.4×10^6 S/m, respectively, which are greater than that of other LMs [2, 4, 5]. The oxide skin allows LM to wet various substrates, and liquid Ga can amalgamate with other metals, enabling the formation of good connection between conductors. However, it is difficult to create homogeneous and mechanically robust thin films of LM covering a large area due to its large surface tension [10]. In addition, Ga forms alloys with metals commonly used in electronics, such as copper, gold, silver, and aluminum, imposing the risk of corroding the circuit [1]. It is also known that residues of LM are commonly deposited within the micro-channel due to the high wettability of the oxide layer. This can be overcome by using an electrolyte such as sodium hydroxide (a solution formed from caustic soda in water). This section has summarized key electrical, thermal, and mechanical properties of various liquid metals. Once we understand the properties of liquid metal the next important consideration is how to actuate (or move) the liquid metal.

III. ACTUATION TECHNIQUES

The most commonly used techniques for actuating LM can be generally categorized as follows: mechanical [12]-[15], magnetic [16]-[19], thermal [20]-[21], and electrical [22]-[34]. The mechanical techniques generally use external pressure to move LM. The pressure may be applied directly to LM using a syringe or a micropump (e.g., Fig. 1(a)). Alternatively, the pressure may be applied via another medium such as air or oil [12]-[14]. The pneumatic approach reguires the use of a pressure regulator and micropump to provide the control. The need for bulky components limits the ability to integrate with RF circuits and antennas. The magnetic technique involves inducing Lorentz force by travelling magnetic fields [16]-[17] and loading the LM with ferromagnetic particles (e.g., Fig.

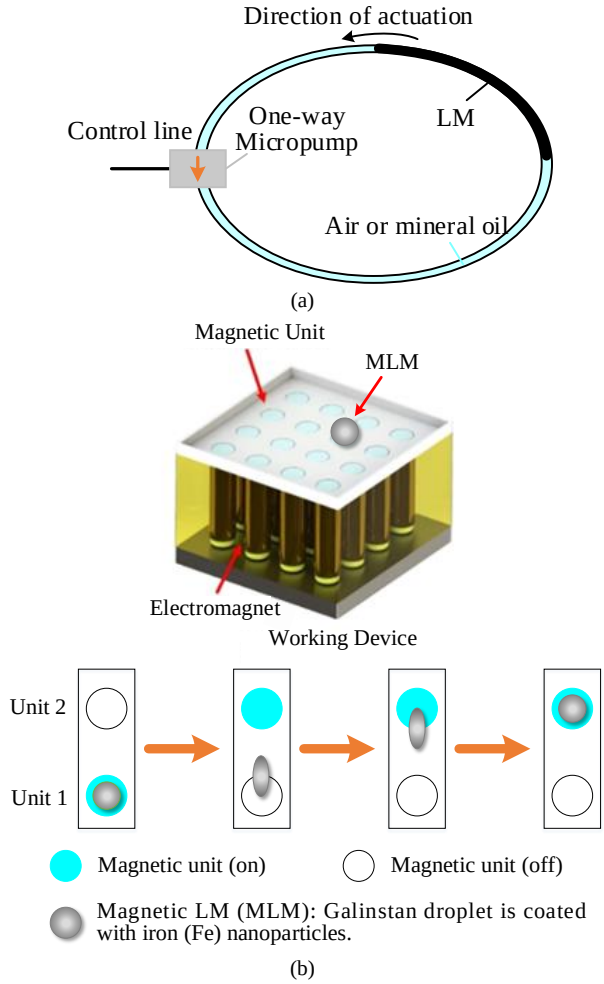

Fig. 1. Actuation of the LM: (a) Mechanical [12]. (b) Magnetic [19].

1(b)) [18]-[19]. However, it usually requires a strong magnetic field which necessitates the use of large currents and thus relatively high power consumption. A change in temperature can also be used to move LM. This technique utilizes the thermal expansion of the LM or of trapped air within the channel to move the LM. Yet, the thermal technique is slow, and a considerable amount of power is consumed within the heating elements [20]. The electrical technique for moving LM utilizes intrinsic properties of the LM. It does not require a bulky pump to produce external pressure, and has the merits of reduced power consumption, miniaturization, and easier integration with other systems. There are four sub-categories of electrical actuation techniques: 1) electrocapillarity [22]-[23], 2) electrowetting on dielectric (EWOD) [24]-[27], 3) continuous electrowetting (CEW) [28]-[32], and 4) electrochemically controlled capillarity (ECC) [33]-[34]. All of these techniques involve manipulating the interfacial tension of LM by applying an electrical potential between a pair of electrodes. Electrocapillary uses reductive electrochemical potentials to remove oxide layer of LM and causes the capillary action of the LM in the capillary. This behavior is also called "recapillarity". The electrocapillary phenomenon can be used to withdraw LM from the capillary [22], as shown in Fig. 2. When the applied potential is removed, the oxide layer rapidly reforms which stops the capillary flow on demand. Fig. 3 illustrates the principle of another electrical actuation technique

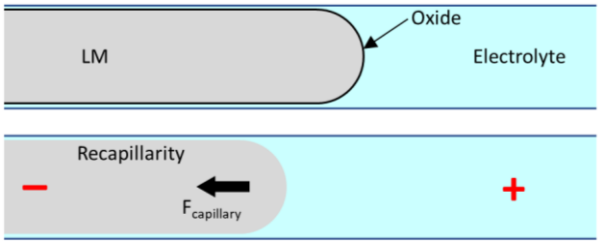

Fig. 2. Electrocapillarity method [22].

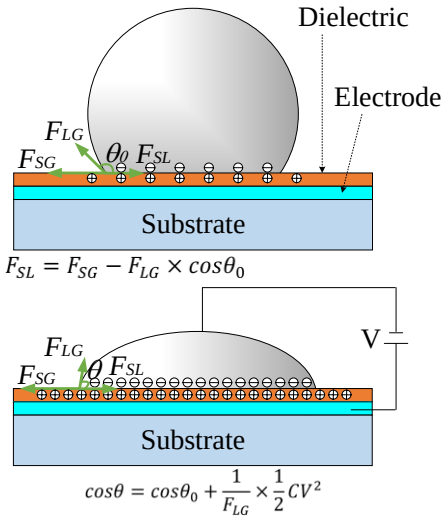

Fig. 3. EWOD method [24]-[25]. C presents the capacitance per unit area, and θ_0 is the contact angle of LM droplet without the electric field across the contact interface. F_{SL}, F_{LG}, and F_{SG} are the solid-liquid surface tension, liquid-gas surface tension, and solid-gas surface tension, respectively. F_{LG} and F_{SG} are presumed to remain constant and unaffected by the applied potential.

- electrowetting on dielectric (EWOD), which is derived from electrocapillarity. In EWOD, an electrical potential is applied between a sharp electrode, inserted into the LM, and a flat electrode, located beneath the LM. A thin layer of insulating material deposited above the flat electrode prevents current flow. The application of an electrical potential alters the equivalent surface energy at the boundary between a liquid and solid insulator interface to generate a driving force, which changes the contact angle of LM droplet [24]-[25]. More specifically, the application of an electrical potential creates an electrostatic fringing field [24]-[25] which flattens the droplet, leading to increased wetting. From the Young's equation, given in Fig. 3, the contact angle decreases as the potential increases. EWOD necessitates the use of a high DC voltage, typically above 100 V, that must be maintained to sustain the deformation of the LM [26]. While EWOD is capable of changing the contact angle of LM droplets, the interfacial behavior is significantly different from conventional liquids due to the presence of a solid oxide layer on the LM surface. This oxide skin, with a thickness of 1-3 nm, causes the LM to adhere to the substrate and mechanically impedes its flow, thereby preventing the droplet from adopting shapes that can minimize the interfacial energy. Consequently, contact angle measurements can be problematic [27]. In dynamic advancing-receding contact angle measurements, the advancing angles (>140°) are consistently much larger than the receding angles,

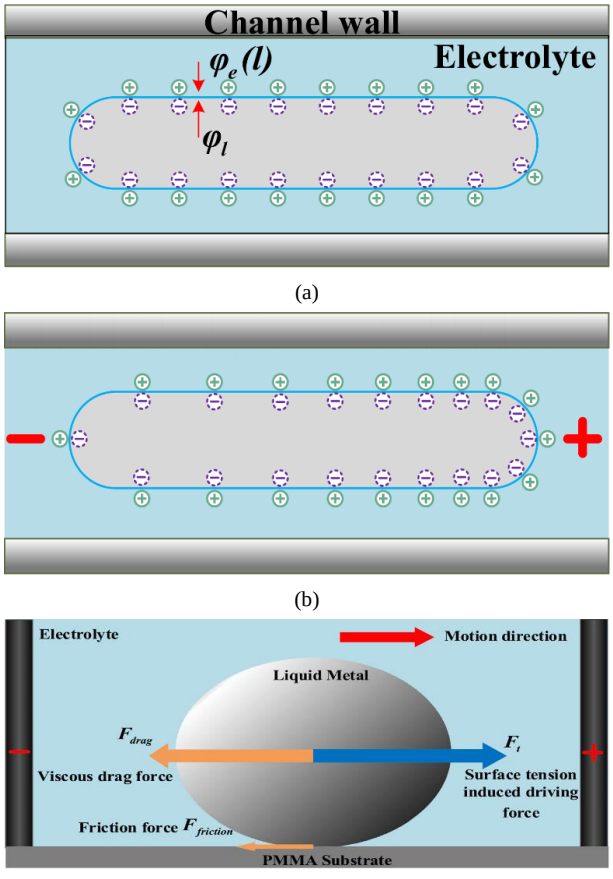

Fig. 4. CEW method [28]. (a) LM droplet with initial charge. (b) Surface charge redistribution upon application of external field. (c) Analysis of forces exerted on a droplet of LM.

regardless of the substrate. This hysteresis in contact angles renders static measurements essentially uninformative [27].

Fig. 4 illustrates the principles of continuous electrowetting (CEW). As with the EWOD method, it also involves applying an electrical potential between a pair of electrodes. However, neither electrode makes direct electrical contact with the LM. Instead, the electrodes are situated within an electrolyte surrounding the LM [28]. The electrolyte is typically sodium hydroxide (NaOH), so no oxide is formed. Application of an electrical potential causes the LM to move towards the positive electrode. Its operation mechanism is as follows: without applied potential, the ionic distribution within the electric double layer (EDL) is uniform, as depicted in Fig. 4(a). Applying an external electrical potential creates a potential gradient within the channel, leading to the redistribution of charges in the EDL, as depicted in Fig. 4(b). This redistribution of charges generates a gradient in surface tension at the LM-electrolyte interface, as per Lippmann's equation, which relates interfacial tension to the density of charge in the EDL. The area with higher surface tension pulls the surrounding liquid with greater force, resulting in Marangoni flows that transport surrounding liquid from the region with lower surface tension towards the region with higher surface tension, as illustrated in Fig. 4(c). This surface flow acts like a conveyer belt that propels the liquid metal droplet towards the anode [29]. Coating the LM droplet's surface with charged nanoparticles can enhance its actuating speed [29]. If the LM droplet is confined, it can serve as a pump to drive the surrounding electrolyte instead of moving the droplet itself [30]. The actuation of LM droplets in electrolytes is feasible with a moderate external potential gradient. An excessively large potential gradient, however, would induce interfacial perturbations at the LM surface, resulting in the expulsion of metals dissolved in Ga, such as tin, indium, bismuth, and zinc, which leads to the formation of metallic and metallic compound nanostructures [31], [32].

Fig. 5 illustrates the principles of electrochemically controlled capillarity (ECC) [33]. Akin with CEW, the method involves applying an electrical potential between a pair of electrodes which are submerged in an electrolyte. Notice that one of the electrodes makes direct electrical contact with the LM. Application of an oxidative electrical potential to LM causes it to stretch. This mechanism can be used to change the length of LM [34]. This behavior can be attributed to the regeneration of a surface oxide layer on the LM. The surface oxide has the effect of reducing the interfacial tension between the metal-oxide and the electrolyte. Increasing the electrical potential reduces the interfacial tension (i.e. the surface tension at the interface between two liquids) at the leading edge of the LM. When the potential reaches a sufficient value, the interfacial tension approaches zero. At this point, the higher Laplace pressure in the reservoir forces the LM to spread towards the negative electrode. Reversing the polarity of the electrical potential electrochemically reduces the oxide layer and returns the LM to a condition of high interfacial tension. The Laplace pressure will eventually draw the LM back into the reservoir, thus shortening the length of the slug. The control is simple, requires less voltage compared with EWOD.

This section discussed various techniques for actuating (i.e., moving) liquid metal. These include: mechanical, magnetic, thermal, and electrical techniques. In summary, each actuation method has its advantages and shortcomings. The selection of the actuation method very much depends on the specific application requirements. Mechanical actuation is simple to implement but its usability may be limited by wear and friction as well as the bulkiness of the actuation system. Magnetic actuation offers fast actuation speeds and can exert large magnetic force, making it suitable for driving heavy LM elements. However, the actuation process is often complicated and vulnerable to external interference due to the application of magnetic fields. Thermal actuation can be precise; however, it may be hampered by slow response time, thermal conductivity, and high-power consumption. Electrical actuation can be both fast and precise, although it may be constrained by the use of electrolyte and accurate electrical control requirements. In general, actuation techniques are very much under-developed for high-frequency circuits and antennas. A lot of the previous work reviewed in this paper focuses on concept demonstrations rather than the practicality and implementation of the actuation. There is still a long a way to go to develop and optimize the

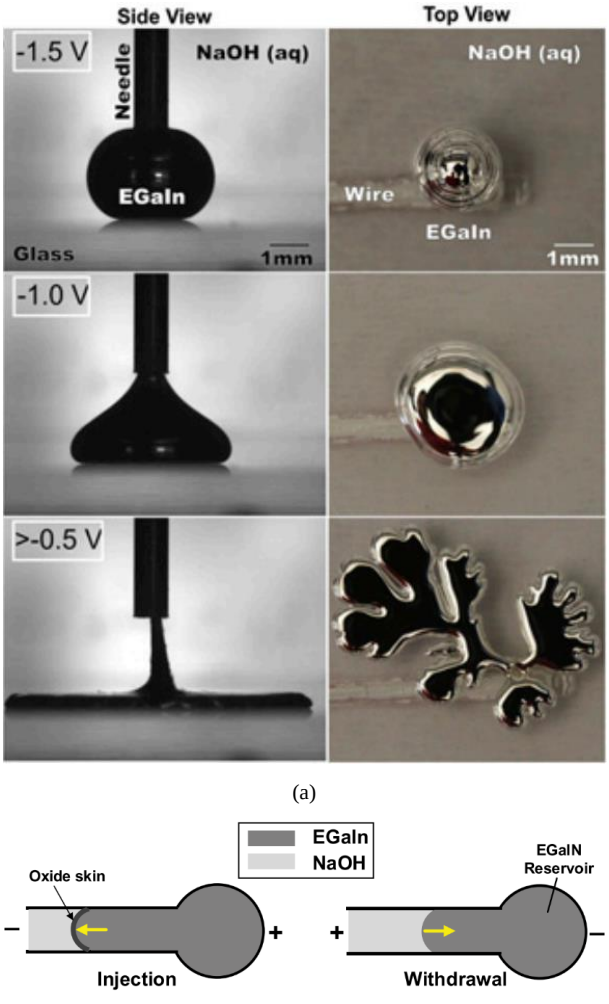

Fig. 5. ECC driving method. (a) Diffusion of LM droplets when voltage is applied [33]. (b) ECC of a slug of EGaIn LM [34].

actuation techniques for circuits and antennas. In order to actuate (or move) the liquid metal we must provide channels in which it can flow, and careful consideration must be given to this topic.

IV. Microfluidic Channels

To contain and control LM, tubes or channels of various sizes and shapes are usually required. Microfluidic channels are often utilized when integration and miniaturization are among the key design drives. Depending on the application, microfluidic channels may be required to have some of the following properties: flexibility and stretchability, impermeability to water and gas, high temperature resistance, resistance to chemical corrosion, low cost, or transparency.

As for the first-generation microfluidic materials, glass and silicon were used for capillary electrophoresis (i.e., the movement of charged particles in a fluid or gel under the influence of an electric field) applications but they are costly for microfabrication [35]-[37]. Elastomers, e.g., PDMS and Ecoflex, allow low-cost rapid microfabrication and high-density integration, making complex fluid manipulation possible [35]-[38]. In recent years PDMS has become one of the most popular materials for fabricating microfluidic channels [40]-[41]. Solid PDMS is a non-toxic, non-flammable, inert, transparent, and elastic polymer which is hydrophobic and water resistant. PDMS has stable chemical properties, excellent biocompatibility, and is easy to combine with a variety of materials. As a substrate, PDMS has a predictable dielectric constant ($\varepsilon_r \approx 2.67$). However, its loss tangent value is high, namely 0.0375 at 77 GHz [41]. This needs to be carefully considered in many high-frequency circuit designs. PDMS microfluidic channels are often manufactured using soft lithography process [40]. A typical process flow is illustrated in Fig. 6. This manufacturing process allows accurate definition of the mold using photoresists, such as SU8, and therefore tight control of the channel dimensions and layouts. For less demanding channel structures, it is also possible to use 3D printing methods [41] or conventional milling techniques to produce the mold for making channels using PDMS or Ecoflex.

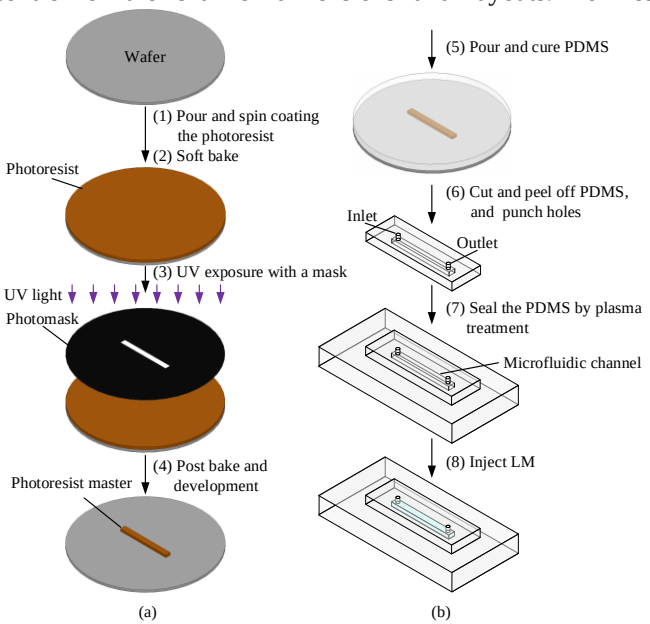

Fig. 6. Fabrication process of the microfluidic channel based on PDMs [40].

Plastics can also be fabricated quickly and cheaply [35]-[37] to form fluidic channels. Their varieties have provided solutions for different demands. For example, thermoplastics, e.g., polymethylmethacrylate (PMMA), polyurethane (PU), polyamide (PI), polyethylene terephthalate (PET), polyvinylidene fluoride (PVDF), and polyvinylchloride (PVC), can be repeatedly reshaped even after curing which is convenient for molding and bonding purposes [35]-[37], whereas some perfluoropolymers, e.g., polytetrafluoroethylene (PTFE), are inert and antifouling [35]-[37].

For the ease of prototyping, glass, silicon, PDMS and Ecoflex are widely used in research laboratories. Polymers such as plastics have gained increased interest in commercial applications due to the low manufacturing costs as well as the ease and reliability of use. In medical and biological applications, silicon, glass, PDMS, Ecoflex and plastics such as PMMA, PU, PI, PET, PVDF, and PTFE are commonly used because of their biocompatibility and other beneficial properties [35]-[38]. Hence, the biocompatibility of Ga-based LM circuits and devices can be ensured if they are encapsulating with these materials.

Next, we will review LM enabled circuits and devices. First, we will consider interconnects and transitions. This is followed by reconfigurable circuits, switches, phase shifters, and antennas, metamaterials. Finally, we will discuss a specific application of the LM technology to flexible, stretchable, and wearable antennas.

V. Interconnects and Transitions

Soft-matter flexible circuits that support bending, stretching, and other kinds of deformations are highly desirable for use in emerging applications, such as wearable computing and soft robotics [42]-[45]. They allow better mechanical matching with other structures while also increasing the resilience of the entire system [42]. For example, soft-matter circuits can be incorporated into garments or placed on the skin. Stretchable electronics can be realized using microfluidic LM traces integrated within elastomers [42]-[45]. LM encapsulated within elastomer channels can be used to form circuits that maintain their electrical properties under deformations and loading conditions [43]. Here, we give some examples of using LM in flexible interconnections. Comprehensive reviews on the general topic of flexible electronic circuits can be found in [46] and [47].

Flexible LM interconnects have been demonstrated in microelectronics [42], incorporating digital and analogue sensors along with surface-mount IC packages. Examples are shown in Fig. 7(a) and (b). A series of quasistatic tensile experiments were performed to determine the strain limit of these circuits. It was found that mechanical failure occurred before electrical failure.

It is highly desirable for some wearable electronics to harvest energy from the environment or the human body for self-powering [44], [45]. EGaIn has been used to create a flexible

thermoelectric generator (TEG) to harvest body heat, as shown in Fig. 7 [45]. Specifically, a standard rigid TEG was converted to a flexible device by replacing the hard ceramic plates and metal connections with stretchable EGaIn [45]. The EGaIn-based interconnects provide not only extremely low interconnect resistance, but also stretchability and self-healing abilities, both of which are critical for flexible electronics.

LM embedded elastomer (LMEE) is another interesting material, based on LM. It is printable and can be used to form 3D structures and circuits. [48] demonstrated a stretchable, flexible, and highly thermally conductive heat sink using 3D-printed LMEE. Fig. 8(a) shows a 3D-printed LMEE breadboard with LED demonstration, and Fig. 8(b) shows how the LMEE can be integrated with a soft wearable TEG which provides heating/cooling to the skin via electrical stimulation [48]. As shown in Fig. 8(c), laser sintering of LM nanoparticles enables the creation of soft and flexible electronics [49]. Electrically conductive patterns are formed through the selective coalescence of liquid metal nanoparticle films using laser beams. In addition, the entanglement of Ag nanowire backbone and dispersed EGaIn can be controlled through laser-induced photothermal reaction, which enables stretchable LM-based conductors to be patterned with spatially programmed strain-resistance characteristics [50]. The nanowire-assisted freestanding, patterned LM thin-film conductor, FS-GaIn, was realized by adding metal nanowires to LM and using selective laser processing and etching to create the desired pattern [51]. FS-GaIn exhibits stability, stretchability, and excellent electrical conductivity, and can be used in non-flat surfaces without extra substrates [51].

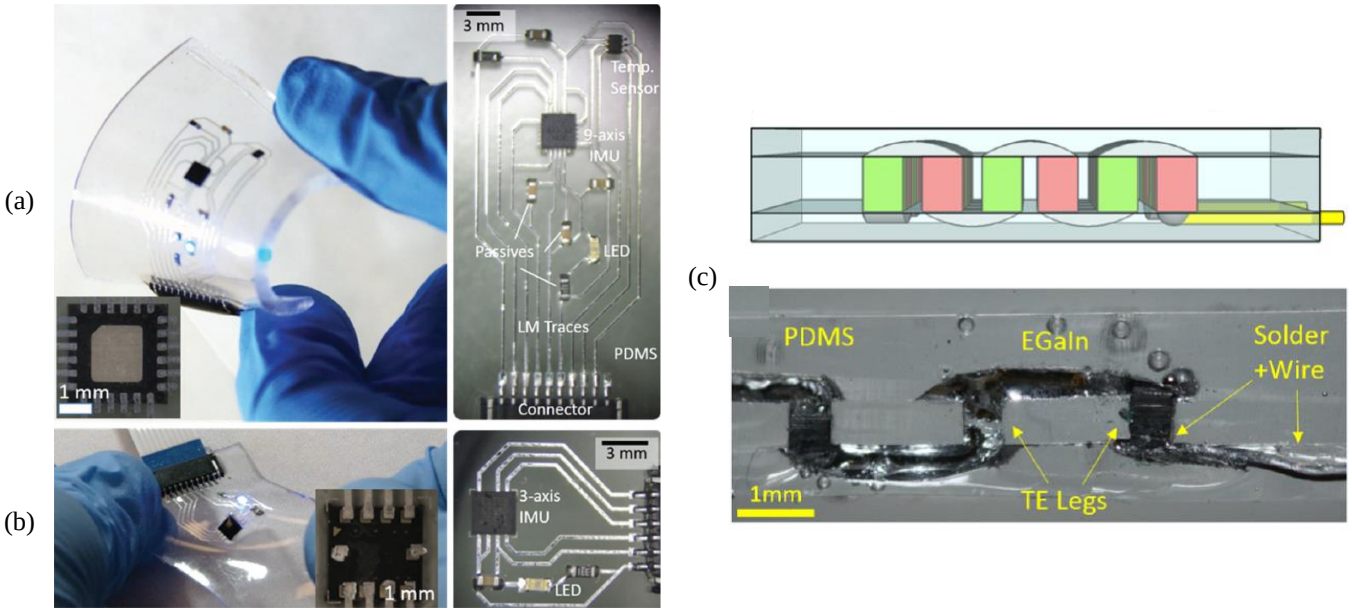

Fig. 7. Examples of stretchable electronic circuits [42] and EGaIn-based flexible TEG [45]. (a) Digital inertial measurement unit and a temperature sensor [42]. (b) Analog accelerometer [42]. (c) EGaIn-based flexible TEG [45].

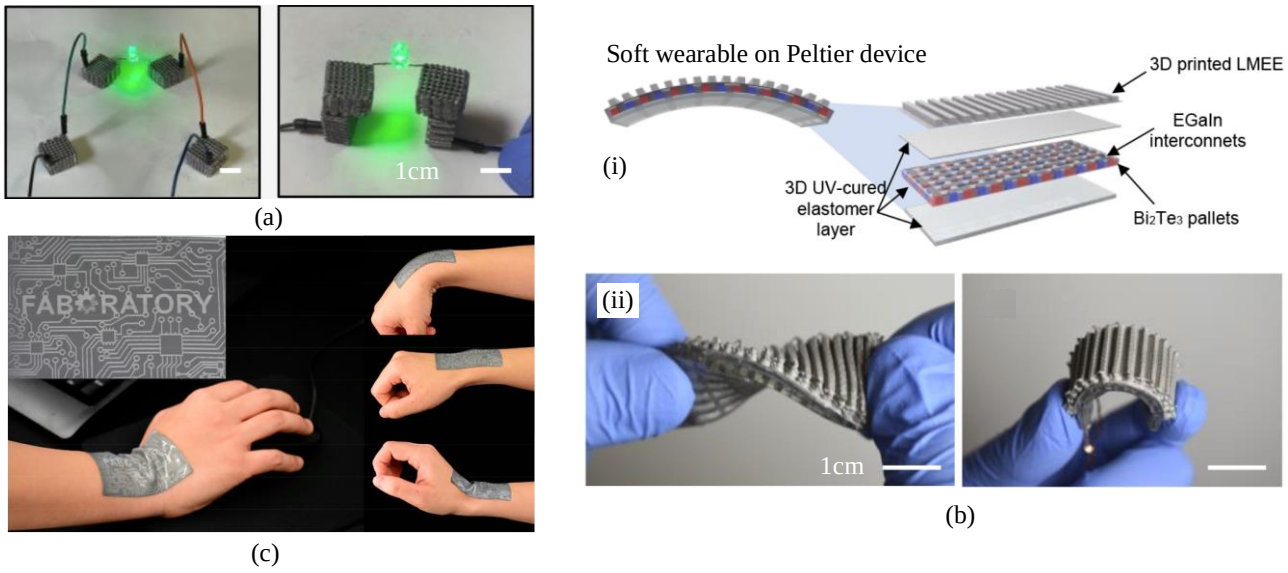

Fig. 8. Flexible devices. (a) 3D-printed LMEE breadboard with LED demonstration. (b) 3D-printed LMEE integrated with wearable TEG. (i) Schematic. (ii) Physical picture [48]. (c) Soft and flexible electronics based on laser-sintered LM nanoparticles [49].

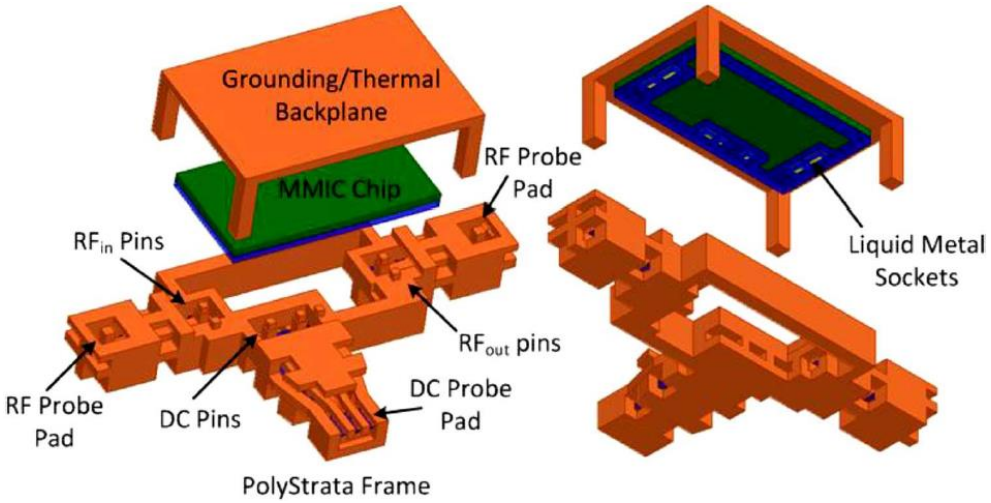

Fig. 9. LM assisted flip-chip assembly [52].

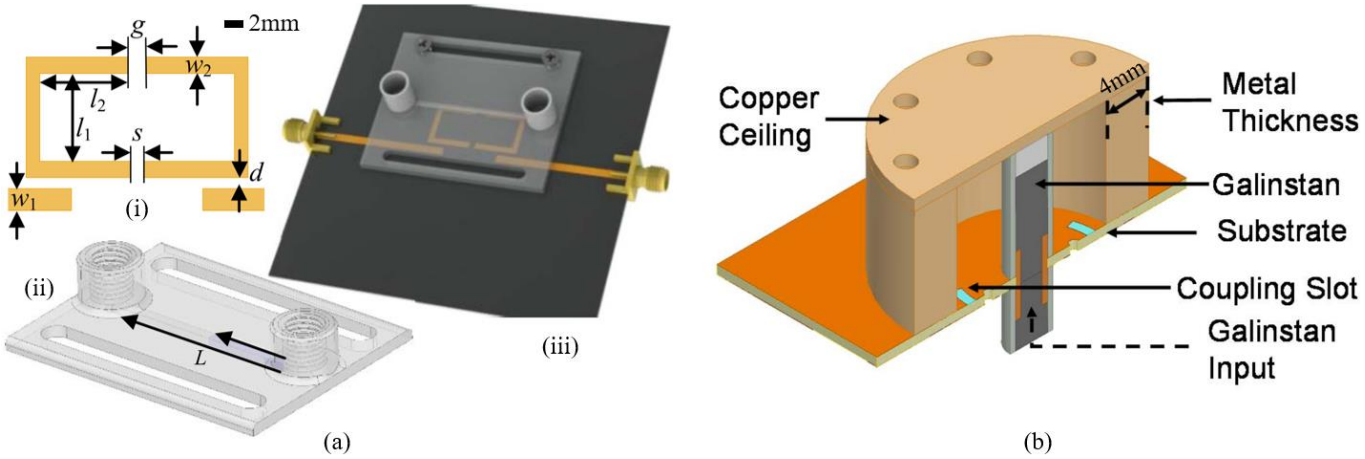

Fig. 10. Reconfigurable resonator. (a) Reconfigurable SRR resonator [54]. (b) Reconfigurable coaxial cavity resonator incorporating a LM post [55].

LM has also been applied as an alternative to wire-bonding, used to interconnect GaAs monolithic microwave integrated circuit (MMIC) chips with 3-D Polystrata transmission-lines [52]. This significantly reduces the parasitic inductance (to ~nH per millimetre of length) associated with the bond wire [53]. An exploded view of the LM transition structure [52] is shown in Fig. 9. The MMIC is attached to the SU-8 structure, which is designed with 'sockets' that keep the LM in place at the bond pad locations. The pins are inserted into the SU-8 sockets and connected to LM. Electrical contact is maintained even when the frame and MMIC expand and shrink at different rates.

This section discussed several examples of interconnects and transitions enabled by LM materials. The flexibility and fluidity of the LM could offer more innovative solutions in circuit connection, packaging and tranmission lines.

VI. Reconfigurable Circuits

A. Resonators

By changing the effective length of a resonator or by altering the volume of LM in a channel, it is possible to adjust the resonant frequency of a resonator [54]. Fig. 10(a) shows a split-ring resonator (SRR). Its resonance frequency is adjusted by altering the length of a parasitic element formed from LM. A programmable pump connected to a syringe was utilized to control the flow rate of LM and achieve acurate and stable control of the LM. Before LM is introduced into the channel, oil is injected as a lubricant to prevent the LM from sticking to the walls of the microfluidic channel. Fig. 10(b) illustrates a coaxial resonator tuned using LM [55]. Its inner conductor is replaced by LM contained within a low-loss Teflon tube. The movement of the LM changes the capacitive gap between the upper wall of the cavity and the apex of the inner conductor and therefore the resonant frequency. Both the inductance and capacitance can be adjusted in this way, allowing wideband tunability.

B. Frequency Reconfigurable Filters

Reconfigurable (also known as tunable) filters are highly desired to create systems that can respond to changes in network conditions or user demand in frequency-agile microwave systems for dynamic spectrum access. Filters are typically formed of multiple coupled resonant circuits such as those microstrip resonators or cavity resonators, discussed in Section VI-A. Similar to resonators, the operating frequency of a filter can be varied by tuning the equivalent capacitance or inductance of the constituent resonant circuits. Parameters that may be tuned include central frequency, bandwidth, and the number of pass/stop bands [56]-[62]. McClung *et al* [58]

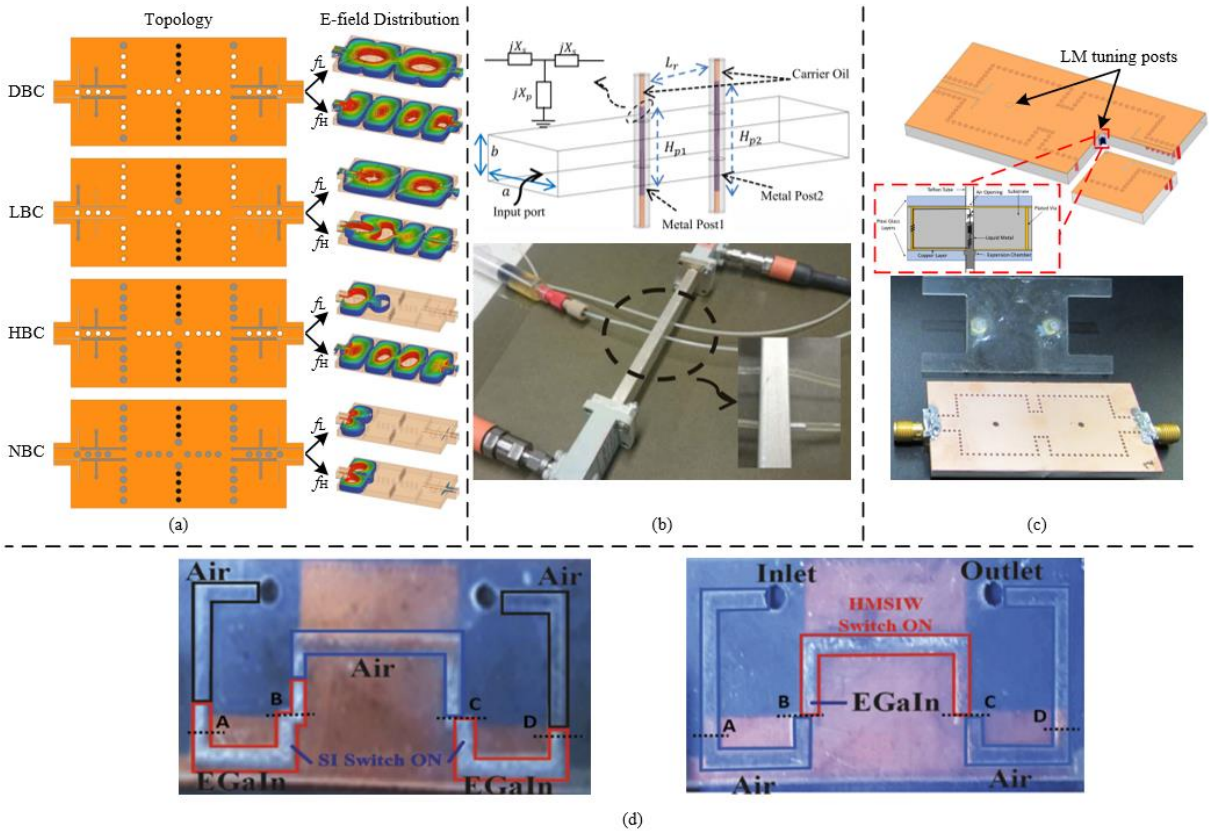

Fig. 11. Reconfigurable/tunable filters based on LMs. (a) A band-reconfigurable filter [58]. (b) A reconfigurable band-reject/1-pole band-pass filter [60]. (c) A 2-pole continuously-tunable bandpass filter [61]. (d) A discrete reconfigurable bandpass filter [62].

presents a cavity filter based on substrate integrated waveguide (SIW) technology. It incorporates a number of drilled holes that can be filled or emptied of LM. When the hole is filled, it forms a via. Using different configuration of the holes creates a band-reconfigurable filter with four operating states (see Fig. 11(a)): dual-band (DBC), low-band (LBC), high-band (HBC), and 'no-band' configurations (NBC). The low- and high-band are caused by the TE_{110} mode and TE_{120} mode, respectively. The insertion loss ranges from 0.73 dB to 1.85 dB for the DBC, LBC and HBC, and the reflection coefficient is less than -16.9 dB at the center frequencies of 4.62 GHz and 7 GHz. This approach involves a large number of LM vias that must be reconfigured in order to change the operating state. It would be desirable to simplify the via implementation and actuation to reduce the complexity. Vahabisani *et al* [60] presents a filter that can be reconfigured between band-reject and band-pass (see Fig. 11(b)). Two LM 'posts' are used. When one post is partially filled with LM, the filter operates in band-reject mode with a bandwith over 18.2 - 21.1 GHz. When both posts are employed, a tunable 1-pole band-pass filter with 2 states is formed. The reflection coefficient is less than -20 dB, while the insertion loss, at center frequency, is 2.3 dB and 2.8 dB for State 1 and State 2, respectively. This design is simpler to reconfigure than that in [58] due to the reduced number of LM posts. However, the tuning range of the band-pass filter is only 0.57%. Pham *et al* [61] presents a 2-pole band-pass filter based on rectangular SIW resonators (see Fig. 11(c)). Its operating frequency can be continuously tuned from 3.3 GHz to 5.8 GHz. This is achieved using LM posts which create capacitive loading in the centre of the waveguide. The loading capacitance can be altered by adjusting the height of the LM posts. The measured insertion loss ranges from 1.5 dB to 7.5 dB, and the fractional bandiwdth (FBW) ranges from 0.68% to 2.33%. The approach of using LM posts for capacitive loading is unsuitable for wideband applications. In fact, most work in the literature relies on either altering the length of LM or filling/emptying LM posts. Park *et al* [62] proposes a different approach which involves changing the width of the transmission line using LM switches. It creates a bandpass filter capable of reconfiguring between a number of discrete frequencies (see Fig. 11(d)). The low- and high-cutoff frequencies of the filter are dictated by the microstrip step impedances (SIs) and the half-mode substrate-integrated waveguide (HMSIW), respectively. A series of channels, which can be filled or emptied of LM, are used to switch the SIs and the HMSIW on and off. When the SI switches are on, the device operates as a band-pass filter within the first operating band at 3.85 GHz and with the FBW of 44%. The average insertion loss is 1.25 dB. When the HMSIW switch is on, the band-pass filter operates within the second operating band at 5.7 GHz with the FBW of 30% and insertion loss of 2.5 dB.

C. Variable Couplers

A variable directional coupler plays an important role in some beam forming antennas [63], as well as in vector sum phase shifters [64]. A variable coupler may also be used in place of the PIN diode in amplitude control circuits. The approach leads to a reduction in the harmonics [65].

Couplers are generally designed using coupled transmission lines located in close proximity to one another. The coupling between the lines can be altered by varying the physical overlap

or separation between them. In [66], LM was utilized to reconfigure a multisection broadband coupler, as shown in Fig. 12. A series of chambers were cut into the dielectric substrate, between the middle pair of strips. Initially the chambers were filled with DialaBX lubricant with a permittivity similar to that of the substrate material and thus preserves the homogeneity of the stripline. When the DialaBX is replaced by LM, the space between the middle pair of strips is effectively reduced, resulting in a change of the coupling [66].

VII. Switches

RF switches are critical components in high-frequency electronic systems. They bridge or block the transmission path and can be used to switch between different circuit states or between multiple signal paths. The main types are: mechanical [67], solid-state (e.g., PIN diode, FET, transistors) [68]-[69], and microelectromechanical systems (MEMS) [70] switches. Mechanical switches offer superior power handling capability compared with other types. However, they are bulky in construction. PIN diode switches are the most widely used. They require DC bias. PIN diodes are nonlinear devices which

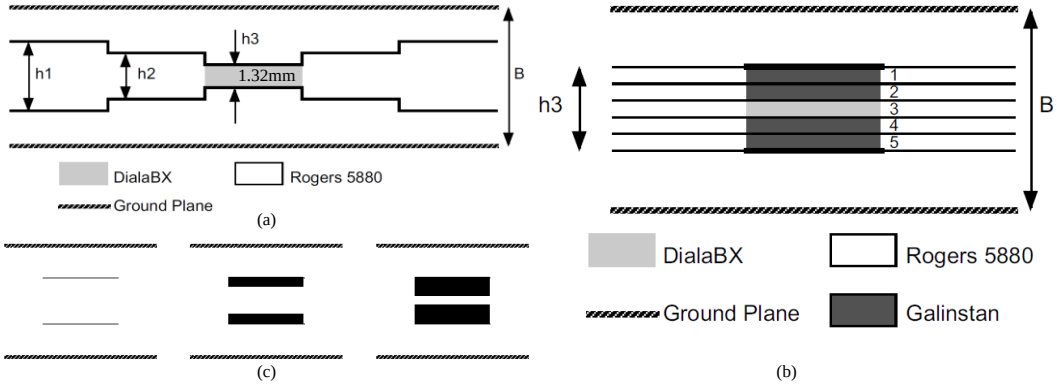

Fig. 12. Variable coupler using LM [66]. (a) Side view of a five-section widerband coupler. (b) Cross-section view of the middle section. (c) Different operating states of the coupler when different numbers of chambers are filled with LM.

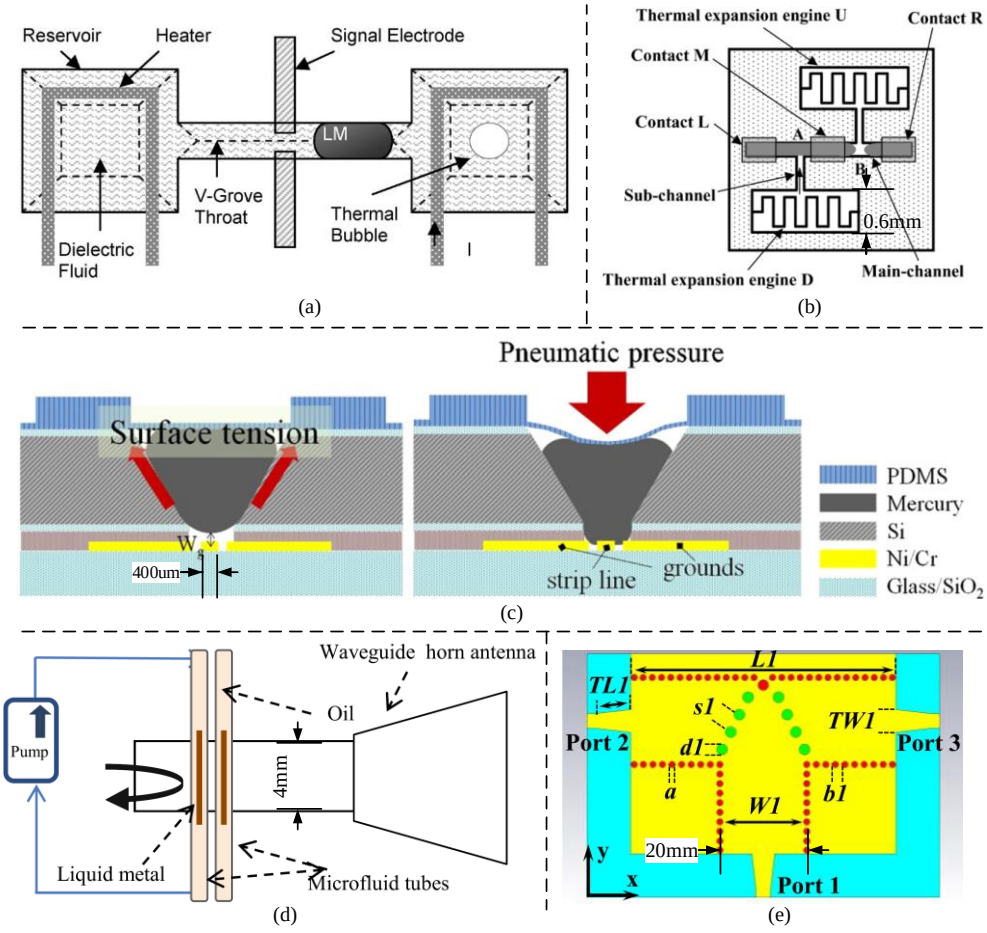

Fig. 13. Switches that are reconfigured using LM. (a) [75] and (b) [76] are thermally actuated, whereas (c) [77], (d) [78], and (e) [79] are actuated using pnumatic pressure.

cause harmonic distortion in circuits and antennas [68]. PIN diodes also have limited power handling capability. While MEMS switches have excellent linear performance, they have poor reliability and usually require very high actuation voltages [70]. Compact and high performance RF switches are in great demand for wireless systems. In 2009, Sen and Kim [71] reviewed the work on microscale liquid-metal switches.

Unlike MEMS, switches employing LM usually do not require high actuation voltages, nor do they require sustained voltage to maintain the switching states. Two approaches have been demonstrated: LM-wetted [71]-[74] and LM-actuated switches [75]-[86]. The former approach involves using LM to coat the contacts of a MEMS switch. The resulting switch is similar to a traditional reed relay [71]-[74]. [72] presents a single-pole single-throw along with a single-pole double- throw switch. These switches employ electrothermal electromagnetic acutation. LM is coated on the solid-solid contacts so as to reduce the contact resistance from 0.3 Ω to 0.015 Ω [72]. The operation of the LM-wetted switch is highly affected by the thinckness of the LM film.

Another way to make a liquid-solid connection is to utilise LM as the moving element within a switch [75]-[86]. In [75], mercury is actuated by a bubble which is driven back and forth by thermal energy (see Fig. 13(a)). When current pass through the heater, the bubble in a reservoir expands and generates sufficient pressure to move the LM droplet. When the LM droplet is positioned over the separated electrodes, the switch is on. The measured contact resistance is about 120 $\Omega/\mu m^2$. The measured switching speed is 10 ms, and the isolation and insertion loss at 2 GHz are 40 dB and 0.1 dB, respectively. Kondoh *et al* [76] reports another thermaly actuated switch (see Fig. 13(b)). When the thermal expansion engine is activated, the gas in the reservoir heats up, causing the pressure within the channel to rise. This forces the LM in the main channel to bridge the gap at switching point B while breaking the contact at point A. The switching speed is 0.92 ms. From dc to 18 GHz, the insertion loss and the isolation were found to be better than 1 dB and 20 dB, respectively. The heater [75] and the thermal expansion engine [76] occupy a relatively large area and consumes a large amount of power. This is not conducive to high levels of integration, or use in low-power devices.

Baek *et al* [77] presents a switch incorporating a LM droplet which moves vertically to make or break the switch (see Fig. 13(c)). In the off-state the droplet is held above the stripline by the surface tension within the droplet. In the on-state, the droplet is pushed against the stripline by 35 kPa of pneumatic pressure, making the connection. At 3 GHz the insertion loss in the on-state is 1.5 dB whereas the isolation in the off-state is 50 dB. Vahabisani *et al* [78] reports a waveguide switch (Fig.

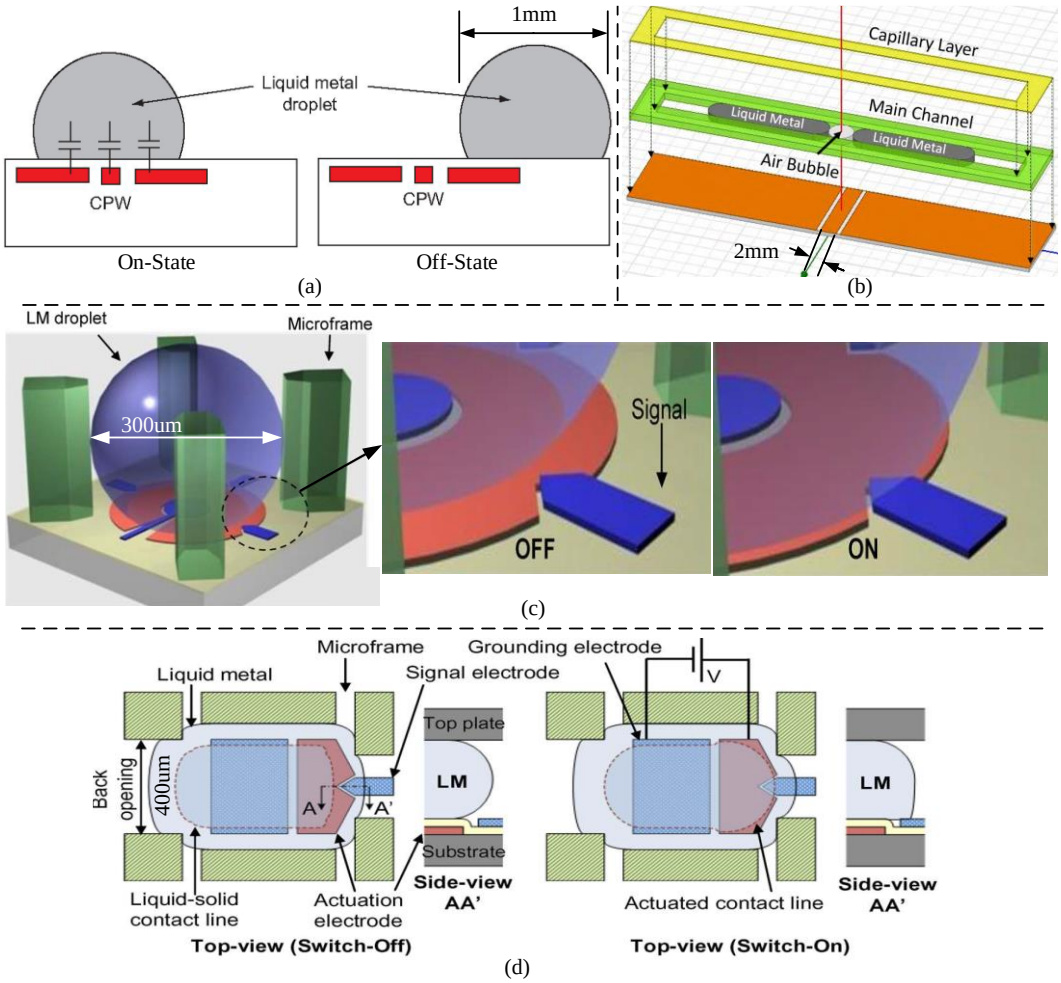

Fig. 14. Electrically actuated LM switches. (a) Electrostatic [80]. (b) CEW [81]. (c) CEW [82]. (d) EWOD [84].

13(d)), formed from a number of tubes which are inserted into a straight section of waveguide. When the tubes are filled with LM they form a wall, and the switch is off. When the tubes are emptied of LM the switch is on. Oil was used to encapsulate the LM. The achieved insertion loss is 0.1 dB and isolation is better than 30 dB at 20 GHz. Alkaraki *et al* [79] presents a SIW single-pole single-throw switch (Fig. 13(e)) in a junction. Each SIW section incorporates an array of drill holes. When filled with LM the holes become vias which block the waveguide. The state of the switch can be changed by filling or emptying selected walls. The insertion loss between two linked ports is 0.7 dB, whereas the isolation between detached ports is 40 dB. The pneumatic means of actuation [77]-[79] requires a syringe or a pressure regulator along with a micropump. This makes it difficult to integrate the switches with other circuits.

Chen *et al* [80] presents a coplanar waveguide (CPW) switch (Fig. 14(a)) that is reconfigured using electrically actuated LM droplet. Electrostatic force induced by a bias voltage between the actuation electrode and LM moves the droplet. From dc to 20 GHz, the insertion loss is less than 0.6 dB, and the isolation is about 15.7 dB at 10 GHz and 21.1 dB at 20 GHz. The actuation voltage is 110 V, which is less suitable for portable device applications. In [81] and [82] (Fig. 14 (b) and (c)), the droplet of LM is actuated by CEW, whereas in [84] the droplet of LM is actuated by EWOD (Fig. 14(d)). Both methods actuate the LM by altering the surface tension and therefore the wetting angle of the droplet. From Section III, the reader will recall that CEW is a low-voltage actuation technique. Nonetheless, the moderate electrical conductivity of the electrolyte means that it would absorb the RF signal if it were brought into contact with the tranmission signal. To combat this problem, air bubbles [82] were inserted between two droplets of LM in the main channel as shown in Fig. 14(b). From dc to 5 GHz, the measured isolation is less than 20 dB, and the insetion loss ranges from 0.2 dB to 1.2 dB. The time required to turn the switch on was 60 μs. Fig. 14(d) [84] shows a liquid-solid contact micro switch based on the EWOD method. In the off-state a droplet of LM is placed on the ground electrode and confined to that area. When a voltage was supplied to the actuation line, the contact angle of the droplet reduces causing it to spread out due to the reduced surfce tension and makes contact with the signal electrode. Under this condition the switch is turned on. From dc-40 GHz, the measured insertion loss is better than 0.3 dB, and the isolation is around 20 dB. This EWOD based actuation method requires a small switching gap, complex microframe structures for positioning the droplet, and a high DC voltage to sustain the switching condition.

VIII. Phase Shifters

Phase shifters are used to change the phase angle of the RF signal either by switching between different delay lines or by changing the propagation properties of the transmission lines or passive components. For example, these properties can be modified by introducing adjustable capacitive or inductive reactance or by changing the length of the transmission line. Tunable phase shifters have been realised using a variety of approaches and technologies, including: MEMS [85]-[88], semiconductors [89]-[91], ferroelectric (a substance for which the strength of the electric polarization varies with the applied electric field) [92]-[97] and liquid crystals (LC) [98]-[101]. LM offers a novel alternative.

Dang *et al* [102] presents a phase shifter based on an electromagnetic bandgap (EBG) structure (Fig. 15(a)). Its phase can be adjusted by using LM to fill or empty holes in the defected ground plane. There are several etched holes with different radii - 1.8 mm, 2.7 mm, and 4.05 mm - providing 1.8°, 5.7°, and 9.4° phase shift, respectively. The average insertion loss is 1.1 dB and the maximum phase shift is approximately 67°. Alkaraki *et al* [103] proposed a SIW phase shifter by employing the switched delay line approach to achieve coarse

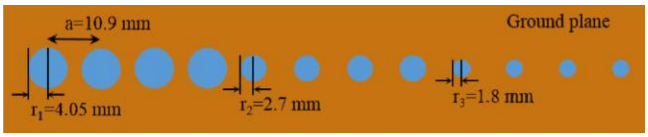

(a)

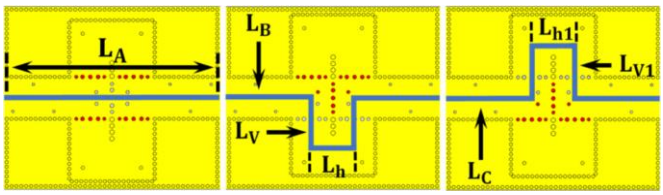

(b)

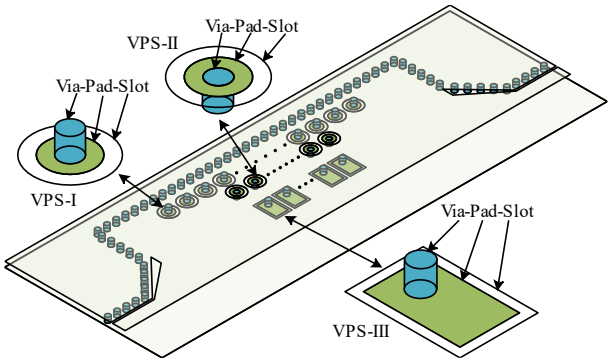

(c)

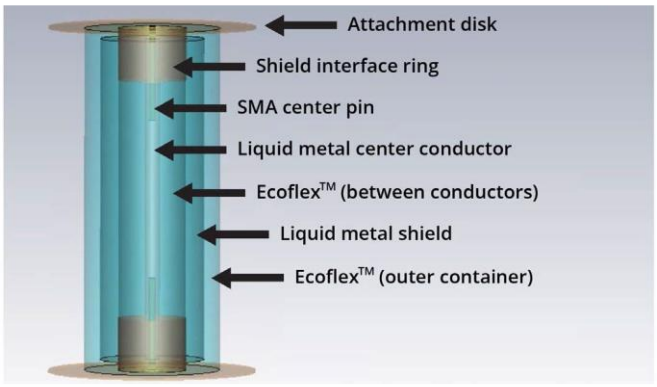

(d)

Fig. 15. Phase shifters. (a) EBG based phase shifter [102]. (b) SIW delay-line phase shifter [103]. (c) VPS based HMSIW phase shifter [104]. (d) Stretchable coaxial phase shifter [105].

phase changes (Fig. 15(b)). The path of the delay line is altered using walls formed from LM vias that can be added or removed. It is possible to switch between one of three pathways, resulting in phase tuning steps of 60°, 120°, and 180°. Fine tuning of the phase, in 10° steps, is achieved by introducing reactive loading into each pathway. The loading is realised using drill holes that can be filled and emptied of LM. Wu *et al* [104] introduced a linear and self-compensating phase shifter based on half-mode substrate-integrated-waveguide (HMSIW), which utilizes a via-pad-slot (VPS) structure. This structure enables phase shift by changing the equivalent shunt capacitance and inductance when the slot is covered with LM (Fig. 15(c)). The phase shifter achieves a phase shift range of 0 - 180°, with an insertion loss of around 1.1 dB, which is almost independent of the phase, and a phase resolution of 1.68º. The key advantage of the VPS structure is its planar strucutre. LM, contained in microfluidic channels, runs on the surface of the SIW structure rather than through the substrate. This not only faciliates the actuation but also introduces minimal insertion loss. Hensley *et al* [105] introduced a streachable coaxial phase shifter, see Fig. 15(d). The centre conductor and outer shield are both formed from LM and housed within flexible Ecoflex™ material. When the coaxial line is stretched, the phase is altered linearly. As both the central and shield diameters deform in the same proportion, the characteristic impedance can be maintained.

Now that we have disucssed LM-enabled reconfigurable passive circuits such as resonators, filters, couplers, switches, and phase shifters, we will move on to the use of LM in antennas.

IX. Reconfigurable Antennas

This section reviews antennas that can be reconfigured using LMs. In reconfigurable antennas, LM is used mainly to: 1) tune the operation frequencies of the antennas. In majority of cases, the resonant frequency is reconfigured by changing the electrical length of the resonator or the electrical length of the radiating element utilizing LM. In some other less common cases, the resonant frequency is reconfigured by changing the length of the ground plane of the antenna, 2) reconfigure antennas radiation patterns. Specifically, LM has been used to alter the antennas main beam directions, or their beamwidths. For example, in Yagi-Uda antenna which is the most widely used antenna structure in this category, the direction of the beam as well as the direction of the null are controlled by altering the location of reflectors and directors. Typically, the reflector, directors or both are formed of LM, 3) reconfigure the polarization of the antenna. This mostly done by changing the shape of the radiator using LM. For example, LM is used to fill/empty four different triangular channels on the edge of the patch antenna, which in return enables the antenna to change its polarization, 4) reconfigure the frequency and polarization of the antennas. This is the least common type of LM reconfigurable antennas. The reconfigurability of frequency and polarization is mainly achieved by changing the size and shape of the two-dimensional structure. For example, a liquid-metal patch shape can be changed, so that switching between different frequencies and different polarization states is achieved.

A. Frequency Reconfigurable Antennas

Frequency reconfigurable antennas can be grouped into two broad categories, namely those providing: (1) continuous frequency tuning, and (2) discrete frequency reconfiguration (also known as frequency switching).

Table II summarizes state-of-the-art of antennas that employ LM to achieve continuous frequency tuning (CFT) [13], [34], [106]-[116]. The majority of these designs operate at below 5 GHz. A handful operate at frequencies up to 10 GHz. The main reason for this limitation on the upper frequency is the challenge associated with the actuation of LM. All of the antennas, featured in Table II, have a relatively low average gain ($\leq$ 6 dBi) and a narrow instantaneous bandwidth (BW $\approx$ 10%) within each tuning step. Most of the antennas are linearly polarized. One of the main advantages of the LM-enabled CFT antennas is that they can support a very wide tuning range that exceeds 2:1 (or 100%), in most cases. In the following, we will consider several examples.

TABLE II

Continuous Frequency Tuning Antenna

Type	Operating Frequency (GHz)	BW (%)	Tuning Ratio (%)	Gain (dBi)	Pol.	Efficiency (%)
Patch [13]	2 ~ 3.5	≈ 6~8	70	≈7	Linear	N.A.
Patch [106]	1.3 ~ 3	< 10	≥300	≈5	Linear	65 ~ 80
Patch [107]	3.21 ~ 10.12	< 10	104	5 ~ 6.9	Linear	62 ~ 82
Patch [108]	1.85 or 2.1	< 8	11.2	5.2	Linear	N.A.
Monopole [34]	0.66 ~ 3.4	≈ 10	500	1.1 ~ 3.4	Linear	41 ~ 70
Monopole [109]	0.78 ~ 2.42	≈ 10	310	-4.8 ~ 2.8	Linear	34 ~ 72
Monopole [110]	1.7 ~ 3.5	< 10	200	2.4 ~ 3.4	Linear	87 ~ 92
Monopole [111]	2.0 ~ 9.5	N.A.	500	≈5.2	Linear	N.A.
Quasi-Yagi dipole [112]	1.8 ~ 2.4	≈ 10	<25	8 ~ 8.5	Linear	N.A.
L-band antenna [113]	1.5 ~ 2	< 15	94	2.9	Linear	94
Planar inverted-F antenna [114]	0.62 ~ 0.76	< 10	<20	NA	Linear	N.A.
Array [115]	1.3 ~ 11	< 10	807	4.9	Linear	54 ~ 82
Slot [116]	1.42 ~ 1.84	≈ 10	26	4.1 ~ 4.8	NA	N.A.

TABLE III

FREQUENCY SWITCHING ANTENNAS

Type	Operating Frequency (GHz)	BW (%)	Gain (dBi)	Efficiency (%)
5 elements Yagi-Uda monopole [117]	2.4 and 3.87	N.A.	6.5 ~ 7.65	N.A.
Monopole Antenna [118]	1.29 ~ 5.17	<7	6.2 ~ 8.6	65 ~ 80
Dual band slot [119]	1.8 ~ 3.1 and 3.2 ~ 5.4 (5 bits)	≈40	1.1 ~ 5.4	78
CPW Slot [120]	2.4, 3.5, and 5.8	<5	1.2 ~ 3.5	N.A.
Magnetoelectric dipole [121]	1.79 ~ 3.85	≈ 20	7.8 ~ 9.3	80
Patch antenna [14]	3.59 ~ 11.69	N.A.	7.2	95
Patch antenna [122]	1.6 ~ 2.4	N.A.	N.A.	N.A.

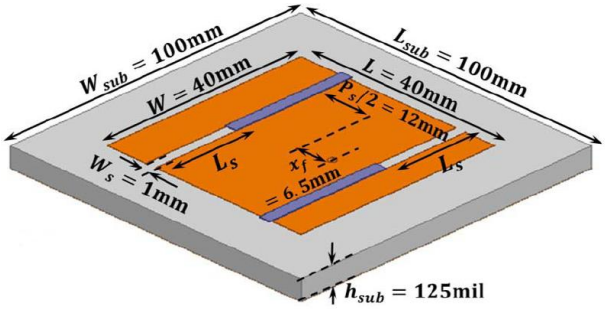

Fig.16. Structure of patch antenna with two tunning slots [13].

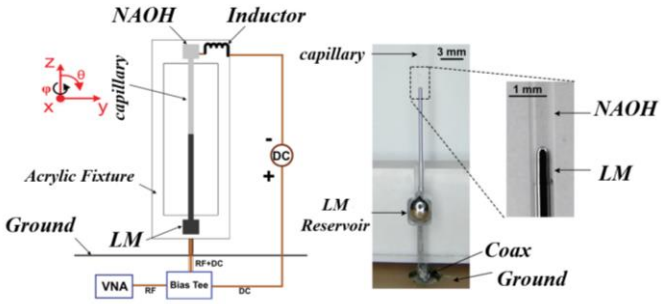

Fig. 17. Schematic and prototype of two tunable monopole antennas [34].

A sizable proportion of the papers, on frequency reconfigurable LM antenna, concern microstrip patch antennas. The resonant frequency is usually reconfigured by altering the effective electrical length of the radiating patch. This can be achieved by changing its physical length [107] or by introducing slots that elongate the resonant current path [108]. By using LM to alter the length of the slot, it is possible to tune the resonant frequency. However, the achievable tuning range is generally relatively modest (<60%) [119]. Another approach is to alter the eigenmode distribution of current on the patch (i.e. the shape of the current distribution). In [13] this was achieved by introducing slots into the radiating patch as shown in Fig. 16. These slots perturb certain eigenmodes (e.g., the TM_{30} mode) and alter their resonant frequency. The slots can be added or removed by filling or evacuating fluidic channels of LM. In this way, it is possible to switch the resonant frequency discretely. Additionally, the length of those slots can be further altered by partially covering them by LM, allowing continuous fine-tuning around each discrete step.

Dipole and monopole antennas are frequently reported because their resonant frequency is directly proportional to their length, and this can be easily changed using LM. Fig. 17 shows

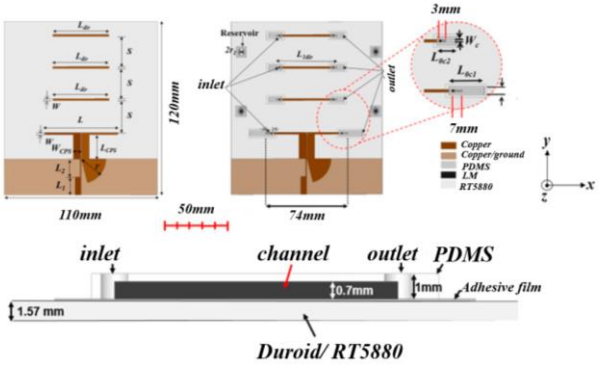

Fig. 18. Frequency-reconfigurable Yagi-Uda antenna [112].

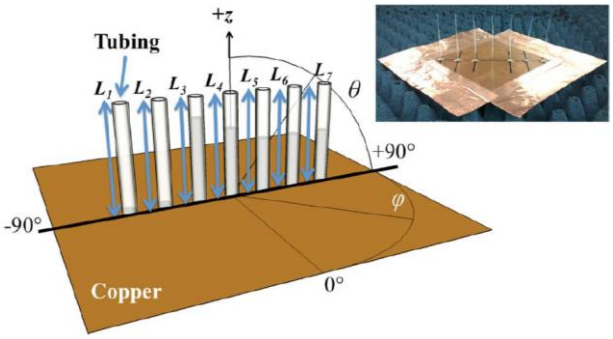

Fig. 19. Reconfigurable Yagi–Uda monopole array antenna incorporating seven elements that can be adjusted using LM [117].

a monopole antenna whose center frequency can be tuned continuously over a very wide range of over 500% [34]. [112] presents a planar Yagi-Uda antenna. The length of the driven element as well as the directors are controlled by injecting LM into fluidic channels, as shown in Fig. 18. Several papers also report frequency reconfigurable LM antennas based on radiating slots. In [116], the frequency of the antenna is tuned by altering the length of the radiating slot and the feed line.

Table III summarizes LM antennas that can switch their resonant frequency between two or more discrete values. Most of these antennas operate at frequencies below 6 GHz, are linearly polarized, have a narrow instantaneous operating bandwidth at each tuning step, and relatively low average gain (below 7 dBi) [117]-[122]. Typically, reconfiguration is achieved by using liquid metal to alter the geometrical structure of the antenna. A variety of different antenna types are employed, including monopoles [117]-[118], slots [119]-[120], dipoles [121], and patches [14], [122]. For example, [117] reports a five-element Yagi-Uda antenna, see also Fig. 19. The antenna consists of a driven monopole located in the center of

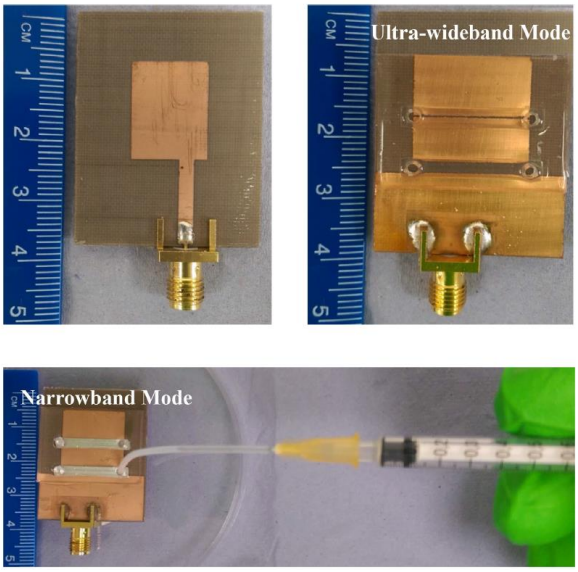

Fig. 20. Frequency switching patch antenna [14].

the antenna, along with six parasitic elements. All the elements are formed from pipes that can be filled to different lengths using LM. Altering the length of the driver tunes the operating frequency. Withdrawing LM from some of the elements will change the number of directors and the antenna gain, whereas altering the length of the parasitic elements located adjacent to the driven monopole could change their function from reflector to director or vice versa. In addition, by switching the location of the reflector and director it is possible to switch the direction of the main beam. [14] shows a patch antenna that can switch its operating bandwidth between ultrawideband and narrowband by connecting/disconnecting the ground plane for the feedline from that of the radiator as shown in Fig. 20. [118] presents a monopole antenna whose length can be tuned between several discrete values. The antenna is fed via a microstrip line which is capacitively coupled to the monopole. A micropump is used to actuate the LM.

[119] and [120] both present slot antennas capable of multi-band operation. Their operating bands can be turned on/off independently by filling and emptying fluidic channels. [122] presents an inset fed microstrip patch antenna that can switch between the 2.4 GHz ISM band and the 1.6 GHz GPS band. The LM is actuated using pressure and moved from a reservoir above the patch.

B. Pattern Reconfigurable Antennas

LM has been used to reconfigure antenna radiation patterns. Specifically, it has been used to alter their main beam directions, or their beamwidths. For the former, there are beam switchable antennas [122]-[131], and continuous beam steerable antennas [12], [132]-[133]. Beam switching is achieved using antennas such as the Yagi-Uda [123]-[128], or a focal plane array [129]-[130]. For the Yagi-Uda antennas [123]-[127], their direction of the beam as well as the direction of the null is controlled by altering the location of reflectors and directors. For instance, the design reported in [125] consists of a driven dipole, fed through a balun. It also incorporates a pair of stretchable parasitic elements implemented using LM. Pattern reconfiguration is achieved by varying the length of the

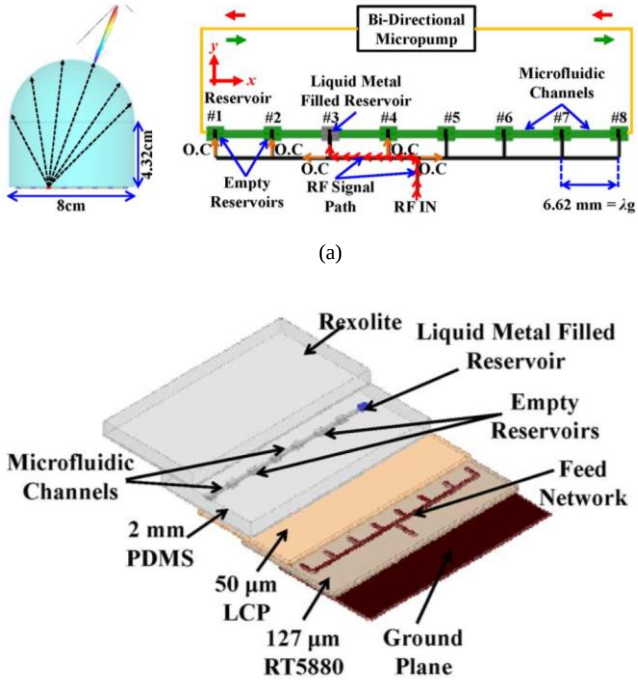

Fig. 21. LM based focal plane array antenna. (a) Conceptual illustration of the array located behind a dielectric lens. (b) Microfluidic structures [129].

parasitic elements. [129] presents a focal plane array antenna placed at the back surface of a lens, as shown in Fig. 21. The array consists of 8 reservoirs. Each reservoir, when filled with LM, acts as a patch antenna. The LM is immersed in low-loss Fluorinert (FC-77). By moving LM using external pump between the reservoirs, the main beam is scanned over a range of $\pm$ 30°. The focal plane arrays, in [129] and [130], are amongst a handful of LM antennas demonstrated at millimeter wave frequencies (e.g., 30 GHz or above).

A limited range of designs provide continuous beam steering [12], [132]-[133]. A novel circular Yagi-Uda array [12], actuated as shown in Fig. 1(a), consists of a driven Alford dipole surrounded by a curved reflector and director. It can steer the beam in fine steps over 360°. The reflector and director can be rotated to face different directions, with the aid of a piezoelectric micropump. The antenna operates at 1.8 GHz and has a 4.0% instantaneous bandwidth. The movable parasitic directors and reflector are implemented using LM injected into a semi-circular fluidic channel. [134]-[137] present antennas that can reconfigure their beamwidth and hence directivity. For example, LM was used in a wired reflector antenna in [135]. This enables the reflector to expand its size in the H-plane and produces controllable and reconfigurable beamwidth.

C. Polarization reconfigurable antennas

Table IV summarizes antennas that use LM to switch their polarization: (1) from linear polarization (LP) to circular polarization (CP) [138], [143], [146]-[147]; (2) between different states of LP (e.g. horizontal and vertical) [139], [140], [141], [144]-[145]; and (3) between left-hand CP (LHCP) and right-hand CP (RHCP) [138], [142], [146]. For example, the patch antenna, proposed in [142] and shown in Fig. 22 operates

TABLE IV

POLARIZATION RECONFIGURABLE ANTENNAS

Type	Frequency (GHz)	Gain (dBi)	Polarization
Slot [138]	2.5	≈7.8	RHCP and LHCP
Dielectric resonator [139]	≈2.7	6	-45°, 45° and 90°
Dielectric resonator [145]	2.2	N.A.	-45° and 45°
Patch [140]	4.3 ~ 5.3	14.4	V and H
Patch [141]	5.19	N.A.	V and H
Patch [142]	2.45	7.3	LHCP and RHCP
Patch [143]	≈1.6	≈6.5	RHCP and LP
Patch [146]	2.45	7	LP, RHCP, LHCP
Patch [147]	3	≈2	LP and CP
Antipodal dipole [144]	≈2.8	1.8 to 2.3	-45° and 45°

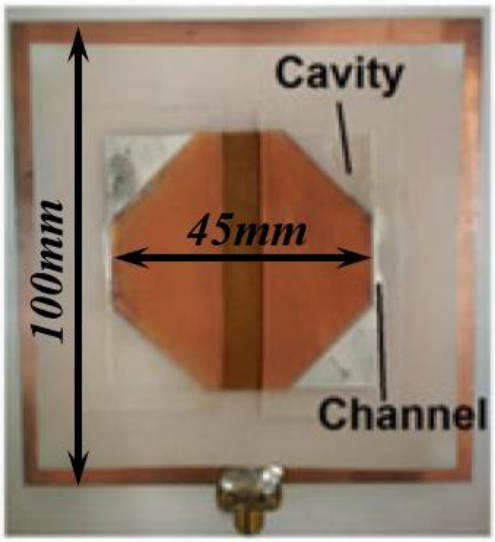

Fig. 22. LM patch antenna in its RHCP State [142].

at 2.45 GHz and can reconfigure its polarization between linear, LHCP and RHCP. Reconfiguration is achieved by filling/emptying 4 different triangular channels at the corners of the patch with LM.

D. Antennas Capable of Reconfiguring both Frequency and Polarization

A multi-parameter reconfigurable antenna is one that is capable of reconfiguring two or more properties (e.g., frequency and polarization, frequency and pattern, etc.) at once. Table V summarizes LM antennas that are capable of providing both frequency and polarization reconfiguration. All [148]-[154] operate at below 5.5 GHz. The types of antennas employed include: dipoles [148]-[149], slots [150], patches [151]-[152], [154] and helices [153]. [151] presents a multi-parameter reconfigurable crossed dipole antenna. Reconfiguration is achieved by varying the length of each dipole arm separately, as shown in Fig. 23. The resonant frequency of each arm can be tuned from 0.8 GHz to 3 GHz. Over a portion of this frequency-tuning band, the polarization of the antenna can be switched from linear to circular. [154] presents a novel pixel array antenna incorporating two-

TABLE V

FREQUENCY AND POLARIZATION RECONFIGURABLE ANTENNAS

Type	Frequency (GHz)	Gain (dBi)	Polarization
Pixelated dual-dipole [148]	1.41, 1.93	-4.41 ~ 2.03	V and H
Dipole [149]	0.8 ~ 3 (LP), 0.89 ~ 1.63 (CP)	0.3 ~ 1.7	LP, CP
Slot [150]	2.03 ~ 2.28 (LP), 2.3 ~ 3 (CP)	2.5 ~ 4	-45° LP, 45° LP, RHCP, LHCP
Patch [151]	2.5 ~ 2.75 (LP), 4.2-4.55 (LHCP, RHCP), 5-5.4 (RHCP)	2.7 ~ 3.7	LP, LHCP, RHCP
Patch [152]	1.6, 2.1, 2.45	1.5 ~ 5	RHCP, LHCP
Helical [153]	1.575	11	RHCP, LHCP
Array [154]	3.61	3.3	H, V

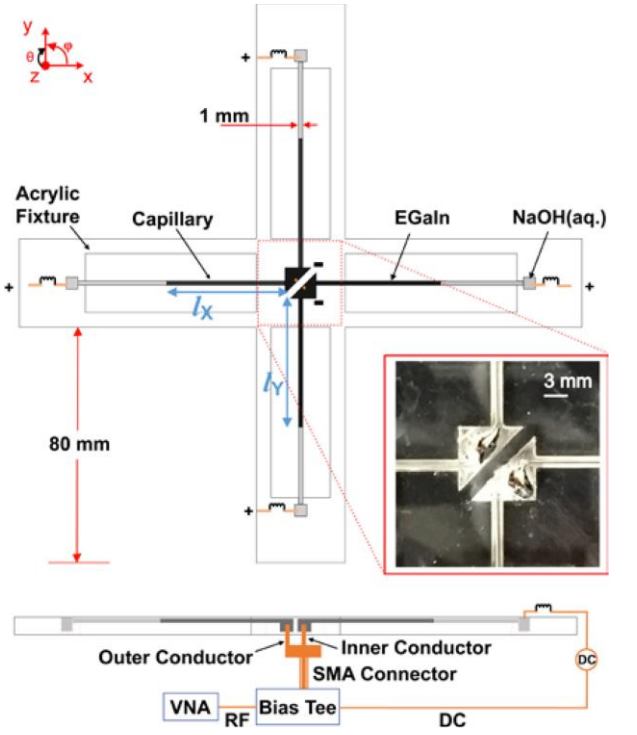

Fig. 23. Schematic of the reconfigurable crossed dipole antenna [151].

dimensional interconnect nodes formed from LM. Reconfigurability is achieved by merging or splitting adjacent nodes to change the size and shape of the two-dimensional structure. The concept is used to create a liquid-metal patch that can be reshaped to switch between different frequencies and LP states. In summary, this section discussed antennas that can reconfigure different performance parameters such as frequency, pattern, polarization, etc. Antenna is one of the most explored areas for using LM. There is still more innovation space due to the unique properties of LM on the one hand and the demand for multi-functional reconfigurable antennas on the other.

X. METAMATERIALS

LM has been used in several metamaterial structures for various applications [155]-[171], such as microwave absorbers

[157]-[163], sensors [164]-[165], antennas and arrays [166]-[167], flexible and reconfigurable metasurfaces [168]-[170] and even THz metamaterials [171]. [160] proposes a switchable metasurface whose absorption spectrum can be switched using LM. It is capable of broadband and polarization-insensitive absorption. Fig. 24 shows the unit cell of the absorber, which consists of a patterned metallisation on the top layer, a flexible substrate, a polydimethylsiloxane substrate, and a metallic ground plane. A microfluidic channel was added with a circular ring capillary and four isolated patches. The absorber comprises of 10×10 cells. The amount of absorption can be reconfigured by filling and emptying the metasurface with LM. When it is empty the absorption is greater than 90%, from 6.23 GHz to 12.14 GHz. When LM is injected into the metasurface, the absorptivity is greater than 90%, from 5.44 GHz to 6.12 GHz

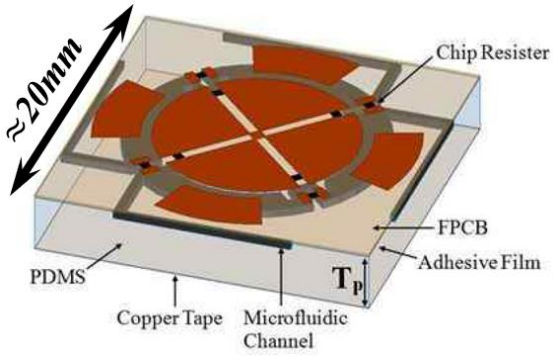

(a)

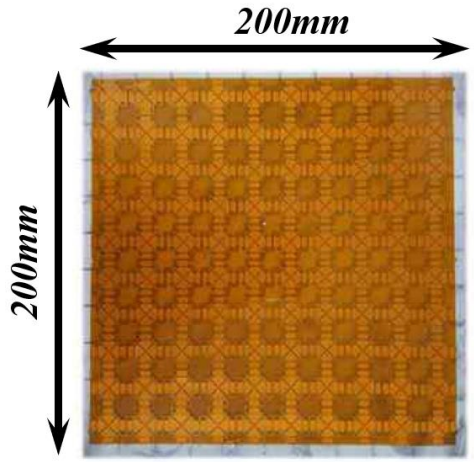

(b)

Fig. 24. Reconfigurable absorber based on LM. (a) Unit Cell and (b) fabricated metasurface with LM [160].

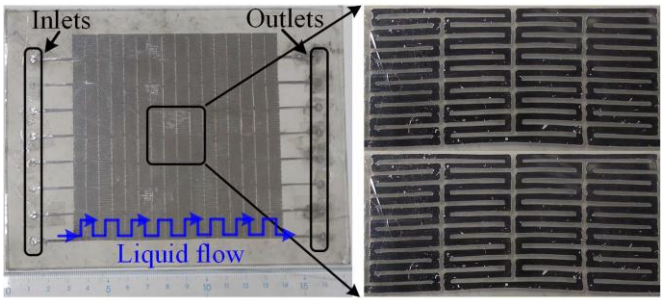

Fig. 25. Frequency selective surface which can be reconfigured using LM [170].

[160]. [170] reports a frequency selective surface (FSS) which can be reconfigured using LM. The surface comprises a meandered channel that is engraved into a flexible dielectric substrate, as shown in Fig. 25. The FSS can switch between two operation modes. The first mode provides band-pass/band-stop performance at 1.36 GHz and 2.63 GHz, when LM is injected into the channel. The second mode provides an all-pass response when LM is withdrawn from the channel [170].

There are opportunities to do more with LM especially with the recent research and development effort on reconfigurable intelligent surfaces (RISs). Traditional tuning elements based on PINs or varactors face significant challenges due to their power consumption and low efficiency. LM offers a new tuning method that can be explored for RISs.

XI. Flexible, Stretchable and Wearable Antennas

The fluidic and pliable nature of LM lends itself the perfect properties for realizing flexible [172]-[179], stretchable [183]-[185] and wearable antennas [178], [180]-[182]. For example, [176] presents a flexible microstrip patch antenna having a multi-layer construction. As shown in Fig. 26, the fluidic channel is formed from an elastomer. When LM is injected into the channel it forms a patch antenna resonating at 3.4 GHz [176]. [178] reports a flexible 3D printed antenna using LM as shown in Fig. 27. It is a miniaturized inverted-F antenna (IFA) operating at 885 MHz, proposed for wearable applications. LM is used to realize the radiating element by filling the channels inside the 3D printed dielectric substrate, used to encapsulate the liquid metal. There are more examples of LM enabled wearable and stretchable antennas of various configurations. One factor that commonly limits the performance (e.g. radiation efficiency in particular) of such antennas is the ohmic loss from the flexible substrates or encapsulating materials due to their

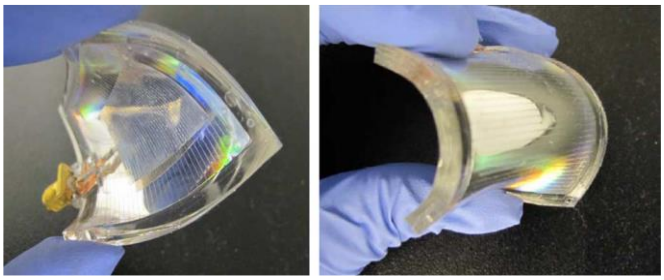

Fig. 26. Flexible patch antenna consisting of LM encased in elastomer [176].

Fig. 27. 3D printed flexible antenna enabled by LM [178].

usually high dielectric loss tangent. This should be one of the major design considerations.

XII. Conclusions

The Ga-based LM has enormous potential for use in reconfigurable circuits and antennas as well as flexible and wearable devices.

Ga-based LMs have enabled many new and novel passive high-frequency circuits, such as interconnects and transitions for flexible circuits, tunable/reconfigurable passive circuits (e.g. resonators, filters, couplers), switches, and phase shifters. The fluidic and shape-shifting properties of the liquid metals can be used to devise innovative tuning or switching structures for enhanced functionalities and frequency agility. The afforded tuning mechanism is largely 'passive' without involving active nonlinear components. This potentially gives the LM-based tuning elements higher power handling capability and better linearity. More comparative studies may be required to establish detailed and deep performance parameters of the LM-based devices beyond the offering of new tuning approaches. For similar reasons, without using active components, liquid metal could also offer advantages in its low loss being akin to a mechanical 'movable' structure in tuning. Diode based tuning elements usually introduce significant insertion losses. A lot can be done to leverage the 'passive' nature of the LM-based tuning elements in overcoming the excessive losses associated with tuning and reconfigurations in circuits such as phase shifters and switches.

LM can be integrated with a wide range of antennas to deliver new and novel capabilities. LM can be used to reconfigure the operating frequency and bandwidth of antennas, their radiation patterns, as well as their polarization. Here the main advantages of using LM include: (1) the ability to achieve wide frequency tuning range, exceeding 100% in many cases and even over 500%; (2) increased capability to achieve multiple parameter reconfiguration, such as changing both the frequency and polarization of the antenna; and (3) the potential to handle higher power than those reconfigurable antennas relying on semiconductor devices [186]. The majority of the reconfigurable antennas based on LM operate at below 5 GHz and few operate at frequencies up to 10 GHz. This is due to the difficulty in containing and actuating LM at high frequencies as the antennas have smaller sizes. Therefore, there is innovation space to extend the LM-based antenna technology to millimetre-wave or even higher frequencies. In addition, LM could also be used with metamaterial structures for microwave absorbers, sensors, and antennas. It is conceivable LM-based tuning mechanism may be applied to reconfigurable metamaterials or intelligent surfaces.

The actuation techniques are the key to the application of LM based devices and the wider adoption of the technology. The non-electric actuation techniques, such as mechanical, magnetic and thermal techniques, require extra motivation equipment to move the LM. These additional bulky components limits the ability to integrate with RF devices. Most electric actuation techniques need electrolyte, which require well-sealed liquid-liquid or liquid-solid systems and cause additional losses. In addition, most electric actuation techniques operate efficiently in strong acidified potassium iodide or base solution, which limits the applications of electric actuation techniques in neutral and non-ionic liquids. When the applied potential difference is higher than 1.2 V, the electrolysis reaction may produce hydrogen bubbles at the cathode, which affects the actuation of LM and reduces the efficiency. A potential approach is to use ionic liquids instead of NaOH solutions [187]. There is still a long way to go in optimizing the actuation techniques for high-frequency circuits and antennas. Important considerations are multifold, such as the footprint and complexity of the actuation systems, the actuation speed (a key parameter for some applications in switches and reconfigurable circuits), controllability (e.g. the precision, accuracy and repeatability in moving liquid metals in microfluidic channels) and reliability. There are certainly no shortage of obstacles and challenges in the development of the technologies. This also means the opportunities are plenty for scientists and engineers from various disciplines.

References

[1] T. Daeneke *et al*, "Liquid metals: fundamentals and applications in chemistry," *Chem. Soc. Rev*., vol. 47, pp. 4073-4111, 2018, doi: 10.1039/c7cs00043j.

[2] N. B. Morley, J. Burris, L.C. Cadwallader, and M.D. Nornberg, "GaInSn usage in research laboratory," *Rev. Sci. Instrum.*, vol. 79 no. 5, pp. 1-3, May 2008, doi: 10.1063/1.2930813.

[3] I. Silverman, A. Arenshtam, D. Kijel, and A. Nagler, "High heat flux accelerator targets cooling with liquid-metal jet impingement," *Nucl. Instrum. Methods Phys. Res. B* 241, pp. 1009–1013, Sep. 2005, doi: 10.1016/j.nimb.2005.07.161.

[4] K. Khoshmanesh *et al*, "Liquid metal enabled microfluidics," *Lab Chip*, vol. 17, pp. 974-993, 2017, doi: 10.1039/c7lc00046d.

[5] M. A. H. Khondoker and A. Ostashek, D. Sameoto, "Fabrication methods and applications of microstructured gallium based liquid metal alloys," *Smart Mater. Struct*., vol. 25, no. 9, pp. 1-23, Aug. 2016, doi: 10.1088/0964-1726/25/9/093001.

[6] T. Y. Liu, P. Sen, and C. Kim, "Characterization of nontoxic liquid-metal alloy Galinstan for applications in microdevices," *J. Microelectromech. Syst*., vol. 21, no. 2, pp. 443-450, April 2012, doi: 10.1109/JMEMS.2011.2174421.

[7] P. Surmann and H. Zeyat, "Voltammetric analysis using a self-renewable non-mercury electrode," *Anal. Bioanal. Chem*., vol. 383, pp. 1009–1013, Oct. 2005, doi: 10.1007/s00216-005-0069-7.

[8] Y. Lin, J. Genzer, and M. D. Dickey, "Attributes, fabrication, and applications of Gallium-based liquid metal particles," *Adv. Sci.*, vol. 7, no. 12, June 2020, doi: org/10.1002/advs.202000192.

[9] D. P. Parekh, C. Ladd, L. Panich, K. Moussa, and M.D. Dickey, "3D printing of liquid metals as fugitive inks for fabrication of 3D microfluidic channels," *Lab Chip*, vol. 16, no. 10, pp. 1812-1820, May. 2016, doi: 10.1039/c6lc00198j.

[10] R. Kramer, C. Majidi, and R. J. Wood, "Masked deposition of gallium-indium alloys for liquid-embedded elastomer conductors," *Adv. Funct. Mater*. Vol. 23, pp. 5292-5296, 2013, doi: 10.1002/adfm.201203589.

[11] D. Youngner, Honeywell AES Technology Centers of Excellence, 2007, private communication.

[12] D. Rodrigo, L. Jofre, and B. A. Cetiner, "Circular beam-steering reconfigurable antenna with liquid metal parasitics," *IEEE Trans. Antennas Propag*., vol. 60, no. 4, pp. 1796-1802, April 2012, doi: 10.1109/TAP.2012.2186235.

[13] L. Song, W. Gao, C. O. Chui, and Y. Rahmat-Samii, "Wideband frequency reconfigurable patch antenna with switchable slots based on liquid metal and 3-D printed microfluidics," *IEEE Trans. Antennas Propag*., vol. 67, no. 5, pp. 2886-2895, May 2019, doi: 10.1109/TAP.2019.2902651.

[14] K. Y. Alqurashi *et al*., "Liquid metal bandwidth-reconfigurable antenna," *IEEE Antennas Wireless Propag. Lett.*, vol. 19, no. 1, pp. 218-222, Jan. 2020, doi: 10.1109/LAWP.2019.2959879.

[15] B. D. Wiltshire, M. A. Rafi, and M. H. Zarifi. "Microwave resonator array with liquid metal selection for narrow band material sensing," *Scientific*

Reports, vol. 11, no.1, pp. 1-8, Apr. 2021, doi: 10.1038/s41598-021-88145-3.

[16] J. Shu, S. Tang, Z. Feng, W. Li, and X. Li, "Unconventional locomotion of liquid metal droplets driven by magnetic fields," *Soft Matter*, vol. 14, no. 35, pp. 7113-7118, 2018, doi: 10.1039/c8sm01281d.

[17] T. Cole and S. Tang, "Liquid metals as soft electromechanical actuators," *Adv. Mater.*, vol. 3, no. 1, pp. 173-185, Nov. 2022, doi: 10.1039/D1MA00885D.

[18] J. Zhang, R. Guo, and J. Liu, "Self-propelled liquid metal motors steered by a magnetic or electrical field for drug delivery," *J. Mater. Chem. B*, vol. 4, no. 32, pp. 5349-5357, 2016, doi: 10.1039/c6tb00996d.

[19] X. Li *et al*., "Programmable digital liquid metal droplets in reconfigurable magnetic fields," *ACS applied materials & interfaces*, vol. 12, no. 33, pp. 37670-37679, 2020, doi: org/10.1021/acsami.0c08179.

[20] J. Simon, S. Saffer, and C.-J. Kim, "A micromechanical relay with thermally-drivenmercury micro-drop," in *Proc. IEEE Conf. Micro ElectroMech. Syst*., San Diego, CA, 1996, pp. 515–520, doi: 10.1109/MEMSYS.1996.494035.

[21] A. Traille *et al*., "A wireless passive RCS-based temperature sensor using liquid metal and microfluidics technologies", *Proc. 41st Eur. Microw. Conf.*, pp. 45-48, Oct. 2011.

[22] M. R. Khan, C. Trlica, and M. D. Dickey, "Recapillarity: electrochemically controlled capillary withdrawal of a liquid metal alloy from microchannels," *Advanced Functional Materials*, vol. 25, no.5, pp. 671-678, 2015, doi: 10.1002/adfm.201403042.

[23] J. A. Lee and I. S. Kang, "Electrocapillarity of an electrolyte solution in a nanoslit with overlapped electric double layer: Continuum approach," *Phys. Rev. E*, vol. 90, pp. 1-9, 2014, doi: 10.1103/PhysRevE.90.032401.

[24] W. C. Nelson, C.-J. 'CJ' Kim, "Droplet actuation by electrowetting-on-dielectric (EWOD): a review," *J. Adhes. Sci. Technol*., vol. 6, pp. 1747-1771, 2012, doi: 10.1163/156856111X599562.

[25] H. Moon, *et al*. "Low voltage electrowetting-on-dielectric," *J. Appl. Phys.*, vol. 92, no. 7, pp. 4080-4087, 2002, doi: org/10.1063/1.1504171.

[26] Y. Damgaci and B. Cetiner, "A frequency reconfigurable antenna based on digital microfluidics," *Lab Chip*, vol. 13, pp. 2883-2887, 2013, doi: 10.1039/c3lc50275a.

[27] I. D. Joshipura *et al*., "Are contact angle measurements useful for oxide-coated liquid metals?," *Langmuir*, vol. 37, no. 37, pp. 10914-10923, Sep. 2021, https://doi.org/10.1021/acs.langmuir.1c01173.

[28] J. Xie *et al*, "Modeling and motion control of a liquid metal droplet in a fluidic channel," *IEEE/ASME Trans. Mech.*, vol. 25, pp. 942-950, 2020, doi: 10.1109/TMECH.2020.2964387.

[29] S.-Y. Tang *et al*, "Electrochemically induced actuation of liquid metal marbles," *Nanoscale*, vol. 5, no. 13, pp. 5949-5957, 2013, doi: 10.1039/C3NR00185G.

[30] S.-Y. Tang *et al*, "Liquid metal enabled pump," *Proceedings of the National Academy of Sciences*, vol. 111, no. 9, pp. 3304-3309, 2014.

[31] M. Mayyas *et al*, "Pulsing liquid alloys for nanomaterials synthesis," ACS nano, vol. 14, no. 10, pp. 14070-14079, 2020, https://dx.doi.org/10.1021/acsnano.0c06724.

[32] M. Mayyas *et al*, "Gallium-based liquid metal reaction media for interfacial precipitation of bismuth nanomaterials with controlled phases and morphologies," Advanced Functional Materials, vol. 32, no. 8, 2108673, 2022, https://doi.org/10.1002/adfm.202108673.

[33] M. R. Khan, C. B. Eaker, E. F. Bowden, and M. D. Dickey, "Giant and switchable surface activity of liquid metal via surface oxidation," *Proc. Natl. Acad. Sci. USA*, vol. 111, no. 39, Sep. 2014, doi: 10.1073/pnas.1412227111.

[34] M. Wang, C. Trlica, M. R. Khan, M. D. Dickey, and J. J. Adams, "A reconfigurable liquid metal antenna driven by electrochemically controlled capillarity," *J. Appl. Phys.*, vol. 117, no. 19, May 2015, doi: 10.1063/1.4919605.

[35] P. Won, S. Jeong, C. Majidi, and S. Ko, "Recent advances in liquid-metal-based wearable electronics and materials," *IScience*, vol. no. 7, 2021 102698, https://doi.org/10.1016/j.isci.2021.102698.

[36] W. Gao, H. Ota, D. Kiriya, K. Takei, and A. Javey, "Flexible electronics toward wearable sensing," Accounts of chemical research, vol. 52, no. 3, pp. 523-533, 2019, https://doi.org/10.1021/acs.accounts.8b00500.

[37] J. B. Nielsen *et al*, "Microfluidics: innovations in materials and their fabrication and functionalization," *Anal Chem.*, vol. 92, no. 1, pp. 150-168, Nov. 2019, https://doi.org/10.1021/acs.analchem.9b04986.

[38] A. Niculescu, C. Chirov, A. C. Bîrcă, and A. M. Grumezescu, "Fabrication and applications of microfluidic devices: A review," *Int. J. Mol. Sci.*, vol. 22, no. 4, pp. 2011, Feb. 2021, https://doi.org/10.3390/ijms22042011.

[39] P. Sen and C.-J. Kim, "Microscale liquid-metal switches—A review," *IEEE Trans. Ind. Electron*., vol. 56, no. 4, pp. 1314–1330, Apr. 2009, doi: 10.1109/TIE.2008.2006954.

[40] Z. Cai, W. Qiu, G. Shao, and W. Wang, "A new fabrication method for all-PDMS waveguides," *Sensors and Actuators A: Physical*, vol. 204, pp: 44-47, 2013, doi: 10.1016/j.sna.2013.09.019.

[41] Y. Huang *et al*, "Microfluidic serpentine antennas with designed mechanical tunability," *Lab Chip*, vol. 14, pp. 4205-4212, 2014, doi: 10.1039/c4lc00762j.

[42] K. B. Ozutemiz, J. Wissman, O. B. Ozdoganlar, and C. Majidi, "EGaIn–metal interfacing for liquid metal circuitry and microelectronics integration," *Adv. Mater. Interfaces*, vol. 5, no. 10, 1701596, pp. 1-13, May 2018, doi: 10.1002/admi.201701596.

[43] I. D. Joshipura, H. R. Ayers, C. Majidi, and M. D. Dickey, "Methods to pattern liquid metals," *J. Mater. Chem. C*, vol. 3, no. 16, pp. 3834-3841, 2015, doi: 10.1039/c5tc00330j.

[44] Y. Sargolzaeiaval *et al*., "Flexible thermoelectric generators for body heat harvesting-Enhanced device performance using high thermal conductivity elastomer encapsulation on liquid metal interconnects," *Appl. Energy*, vol. 262, 114370, pp. 1-13, Mar. 2020, doi: 10.1016/j.apenergy.2019.114370.

[45] F. Suarez *et al.*, "Flexible thermoelectric generator using bulk legs and liquid metal interconnects for wearable electronics," *Appl. Energy*, vol. 202, pp. 736-745, Sep. 2017, doi: 10.1016/j.apenergy.2017.05.181.

[46] M. Zhang, X. Wang, Z. Huang, and W. Rao, "Liquid metal based flexible and implantable biosensors," *Biosensors*, vol. 10, no. 11: 170, 2020, doi:org/10.3390/bios10110170.

[47] Y. Ren, X. Sun, and J. Liu. "Advances in liquid metal-enabled flexible and wearable sensors," *Micromachines*, vol. 11, no .2: 200, 2020, doi: org/10.3390/mi11020200.

[48] P. Won *et al*., "3D printing of liquid metal embedded elastomers for soft thermal and electrical materials," *ACS Appl. Mater. Interfaces*, vol. 14, no. 49, pp. 55028-55038, Dec. 2022, https://doi.org/10.1021/acsami.2c14815.

[49] S. Liu *et al*., "Laser sintering of liquid metal nanoparticles for scalable manufacturing of soft and flexible electronics," *ACS Appl. Mater. Interfaces*, vol. 10, no. 33, pp. 28232-28241, Jul. 2018, https://doi.org/10.1021/acsami.8b08722

[50] C. Cho *et al*., "Monolithically programmed stretchable conductor by laser-induced entanglement of liquid metal and metallic nanowire backbone," Small, vol. 18, no. 37, pp. 2202841, Jul. 2022, https://doi.org/10.1002/smll.202202841.

[51] Kim, Minwoo *et al*, "Nanowire-assisted freestanding liquid metal thin-film patterns for highly stretchable electrodes on 3D surfaces," *npj Flexible Electronics*, vol. 6 no. 1, 99, 2022, https://doi.org/10.1038/s41528-022-00232-1.

[52] P. Ralston, M. Oliver, K. Vummidi, and S. Raman, "Liquid-metal vertical interconnects for flip chip assembly of GaAs C-band power amplifiers onto micro-rectangular coaxial transmission lines," *IEEE J. Solid-State Circuits*, vol. 47, no. 10, pp. 2327-2334, Oct. 2012, doi: 10.1109/JSSC.2012.2204930.

[53] Z. Feng, W. Zhang, B. Su, K. C. Gupta, and Y. C. Lee, "RF and mechanical characterization of flip-chip interconnects in CPW circuits with underfill," *IEEE Trans. Microwave Theory Tech*., vol. 46, pp. 2269–2275, Dec. 1998, doi: 10.1109/22.739210.

[54] M. A. Rafi, B. D. Wiltshire, and M. H. Zarifi, "Wideband tunable modified split ring resonator structure using liquid metal and 3-D printing," *IEEE Microw. Wireless Compon. Lett.*, vol. 30, no. 5, pp. 469-472, May 2020, doi: 10.1109/LMWC.2020.2980740.

[55] K. Sadasivan and D. Psychogiou, "Widely-Reconfigurable 2.5:1 Coaxial-Cavity Resonators Using Actuated Liquid-Metal Posts," 2019 49th European Microwave Conference (EuMC), pp. 300-303, 2019, doi: 10.23919/EuMC.2019.8910873.

[56] B. Lee, B. Koh, S. Nam, T. Lee, and J. Lee, "Band-switchable substrate-integrated waveguide resonator and filter," *IEEE Trans. Microw. Theory Techn.*, vol. 66, no. 1, pp. 147-156, Jan. 2018, doi: 10.1109/TMTT.2017.2737989.

[57] A. C. Guyette, "Intrinsically switched varactor-tuned filters and filter banks," *IEEE Trans. Microw. Theory Techn.*, vol. 60, no. 4, pp. 1044-1056, April 2012, doi: 10.1109/TMTT.2012.2184131.

[58] S. N. McClung, S. Saeedi, and H. H. Sigmarsson, "Band-reconfigurable filter with liquid metal actuation," *IEEE Trans. Microw. Theory Techn.*, vol. 66, no. 6, pp. 3073-3080, June 2018, doi: 10.1109/TMTT.2018.2823307.

[59] J. H. Dang, R. C. Gough, A. M. Morishita, A. T. Ohta, and W. A. Shiroma, "A tunable x-band substrate integrated waveguide cavity filter using

reconfigurable liquid-metal perturbing posts," *IEEE MTT-S Int. Dig.*, pp. 1-4, May 2015, doi: 10.1109/MWSYM.2015.7167060.

[60] N. Vahabisani, S. Khan, and M. Daneshmand, "Microfluidically Reconfigurable Rectangular Waveguide Filter Using Liquid Metal Posts," *IEEE Microw. Wireless Compon. Lett.*, vol. 26, no. 10, pp. 801-803, Oct. 2016, doi: 10.1109/LMWC.2016.2605450.

[61] A. H. Pham, S. Saeedi and H. H. Sigmarsson, "Continuously-Tunable Substrate Integrated Waveguide Bandpass Filter Actuated by Liquid Metal," *IEEE MTT-S Int. Microw. Symp. Dig.*, pp. 21-23, 2019, doi: 10.1109/MWSYM.2019.8700809.

[62] E. Park, M. Lee, R. Phon, and S. Lim, "A multiple liquid metal switching mechanism in a single flow microfluidic channel as a reconfigurable bandpass filter," *Phys. Fluids*, vol. 32, no. 10,102002, 2020, doi.org/10.1063/5.0021644.

[63] K. Ghorbani, A. Mitchell, R. B. Waterhouse, and M. W. Austin, "A novel wide-band tunable RF phase shifter using a variable optical directional coupler," *IEEE Trans. Microw. Theory Techn.*, vol. 47, no. 5, pp. 645-648, May 1999, doi: 10.1109/22.763169.

[64] L. A. Bui, A. Mitchell, K. Ghorbani and T. -H. Chio, "Wideband RF photonic vector sum phase shifter", *Electron. Lett.*, vol. 39, no. 6, pp. 536-537, 2003, doi: 10.1049/el:20030332.

[65] K. Sun, M. Choi, and D. Weide, "A PIN diode controlled variable attenuator using a 0-dB branch-line coupler," *IEEE Microw. Wireless Compon. Lett.*, vol. 15, no. 6, pp. 440-442, June 2005, doi: 10.1109/LMWC.2005.850568.

[66] S. Niyogi, J. Scott and K. Ghorbani, "A novel wideband variable coupler employing liquid metal," *Asia-Pacific Microwave Conference 2011*, pp. 1146-1149, 2011.

[67] X. Li, Z. Yao, L. Zhou, and S. Zhou, "Dispersed operating time control of a mechanical switch actuated by an ultrasonic motor," J*ournal of Vibroengineering*, vol. 20, no. 1, pp. 321-331, 2018, doi.org/10.21595/jve.2017.18234.

[68] P. Sun, *et al*. "A novel SiGe PIN diode SPST switch for broadband T/R module," *IEEE microwave and wireless components letters*, vol. 17, no.5, pp: 352-354, May 2007, doi: 10.1109/LMWC.2007.895706.

[69] K. Maruhashi, H. Mizutani, and K. Ohata, "Design and performance of a Ka-band monolithic phase shifter utilizing nonresonant FET switches," *IEEE Trans. Microw. Theory Techn.*, vol. 48, no. 8, pp. 1313-1317, Aug. 2000, doi: 10.1109/22.859475.

[70] G. M. Rebeiz, C. D. Patel, S. K. Han, C. Ko, and K. M. J. Ho, "The search for a reliable MEMS switch," *IEEE Microwave Mag*., vol. 14, no. 1, pp. 57-67, Jan.-Feb. 2013, doi: 10.1109/MMM.2012.2226540.

[71] S. Kumar, P. Bhushan, M. Pandey, and S. Bhattacharya, "Additive manufacturing as an emerging technology for fabrication of microelectromechanical systems (MEMS)," *Journal of Micromanufacturing*, vol. 2, no. 2, pp. 175-197, 2019, doi: 10.1177/2516598419843688.

[72] A. Cao, P. Yuen, and L. Lin, "Microrelays with bidirectional electrothermal electromagnetic actuators and liquid metal wetted contacts," *Journal of microelectromechanical systems*, vol. 16, no. 3, pp: 700-708, June 2007, doi: 10.1109/JMEMS.2007.893520.

[73] A. Cao, J. Kim, and L. Lin, "Bi-directional electrothermal electromagnetic actuators," *Journal of Micromechanics and Microengineering*, vol. 17, no. 5, pp: 975-982, May 2007, dio: 10.1088/0960-1317/17/5/018.

[74] J. Simon, S. Saffer, F. Sherman, and C. J. Kim, "Lateral polysilicon microrelays with a mercury microdrop contact," *IEEE Transactions on Industrial Electronics*, vol. 45 no. 6, pp: 854-860, Dec. 1998, doi: 10.1109/41.735328.

[75] J. Simon, S. Saffer and C.-J. Kim, "A liquid-filled microrelay with a moving mercury microdrop", *J. Microelectromech. Syst.*, vol. 6, no. 3, pp. 208-216, Sep. 1997, doi: 10.1109/84.623109.

[76] Y. Kondoh, T. Takenaka, T. Hidaka, G. Tejima, Y. Kaneko and M. Saitoh, "High-reliability high-performance RF micromachined switch using liquid metal", *J. Microelectromech. Syst.*, vol. 14, no. 2, pp. 214-220, Apr. 2005, doi: 10.1109/JMEMS.2004.839604.

[77] S. Baek, U. Park, I. H. Choi, and J. Kim, "Pneumatic RF MEMS switch using a liquid metal droplet," *J. Micromech. Microeng*., vol. 23, no. 5, May 2013.

[78] N. Vahabisani, S. Khan, and M. Daneshmand, "A K-Band Reflective Waveguide Switch Using Liquid Metal," *IEEE Microw. Wireless Compon. Lett.*, vol. 16, pp. 1788-1791, 2017, doi: 10.1109/LAWP.2017.2679072.

[79] S. Alkaraki, J. Kelly, A. L. Borja, R. Mittra, and Y. Wang, "Gallium-based liquid metal substrate integrated waveguide switches," *IEEE Microw. Wireless Compon. Lett.*, vol. 31, no. 3, pp. 257-260, March 2021, doi: 10.1109/LMWC.2020.3040795.

[80] C. -h. Chen and D. Peroulis, "Electrostatic Liquid-Metal Capacitive Shunt MEMS Switch," 2006 IEEE MTT-S International Microwave Symposium Digest, 2006, pp. 263-266, doi: 10.1109/MWSYM.2006.249483.

[81] M. R. Moorefield, R. C. Gough, A. T. Ohta, and W. A. Shiroma, "An electrically actuated DC-to-11-GHz liquid-metal switch," *IEEE Access*, vol. 6, pp. 1261-1266, 2018, doi: 10.1109/ACCESS.2017.2778184.

[82] P. Sen and C. Kim, "A fast liquid-metal droplet microswitch using EWOD-driven contact-line sliding," *J. Microelectromech. Syst.*, vol. 18, no. 1, pp. 174-185, Feb. 2009, doi: 10.1109/JMEMS.2008.2008624.

[83] P. Sen and Chang-Jin "CJ" Kim, "A fast liquid-metal droplet switch using EWOD," in *Proc. IEEE 20th Int. Conf. MEMS*, Kobe, Japan, pp. 767-770, doi: 10.1109/MEMSYS.2007.4432998.

[84] P. Sen and C. Kim, "A liquid–solid direct contact low-loss RF micro switch," *J. Microelectromech. Syst*., vol. 18, no. 5, pp. 990-997, Oct. 2009, doi: 10.1109/JMEMS.2009.2029170.

[85] K. Topalli, Ö. A. Civi, S. Demir, S. Koc, and T. Akin, "A monolithic phased array using 3-bit distributed RF MEMS phase shifters," *IEEE Trans. Microw. Theory Techn.*, vol. 56, no. 2, pp. 270-277, Feb. 2008, doi: 10.1109/TMTT.2007.914377.

[86] G. M. Rebeiz, G. L Tan, and J. S. Hayden, "RF MEMS phase shifters: Design and applications," *IEEE Microwave Mag*., vol. 3, no. 2, pp. 72–81, June 2002.

[87] G. Anitha and K. Kiran, "Miniaturized switched line MEMS phase shifter", *Microw. Opt. Technol. Lett.*, vol. 61, no. 6, pp. 1526-1531, Jun. 2018.

[88] B. Pillans *et al*., "Advances in RF MEMS phase shifters from 15 GHz to 35 GHz", *IEEE MTT-S Int. Microw. Symp. Dig.*, pp. 1-3, Jun. 2012, doi: 10.1109/MWSYM.2012.6258286.

[89] M. Teshiba, R. Van Leeuwen, G. Sakamoto, and T. Cisco, "A SiGe MMIC 6-bit PIN diode phase shifter," *IEEE Microw. Wireless Compon. Lett.*, vol. 12, no. 12, pp. 500-501, Dec. 2002, doi: 10.1109/LMWC.2002.805534.

[90] J. R. De Luis and F. De Flaviis, "A reconfigurable dual frequency switched beam antenna array and phase shifter using PIN diodes," in *Proc. IEEE Antennas and Propagation Society Int. Symp*., pp. 1–4, 2009, doi: 10.1109/APS.2009.5171578.

[91] R. Coats, J. Klein, S. D. Pritchett and D. Zimmermann, "A low loss monolithic five-bit PIN diode phase shifter," in *Proc. IEEE Antennas and Propagation Society Int. Symp.*, pp. 915-918 vol. 2, 1990, doi: 10.1109/MWSYM.1990.99727.

[92] H. Yoon, K. J. Vinoy, J. K. Abraham, and V. K. Varadan, "CPW phase shifter using barium strontium titanate thin film on silicon substrate," in *Proc. IEEE Antennas Propag. Soc. Int. Symp*., vol. 3, pp. 970–972, 2003, doi: 10.1109/APS.2003.1220072.

[93] J. H. Leach *et al*. "Electrically and magnetically tunable phase shifters based on a barium strontium titanate-yttrium iron garnet layered structure," *Journal of Applied Physics*, vol. 108, no. 6, 064106, 2010, doi: 10.1063/1.3486463.

[94] F. Zimmermann, M. Voigts, C. Weil, R. Jakoby, P. Wang, W. Menesklou, E. IversTiffee, "Investigation of barium strontium titanate thick films for tunable phase shifters," *J. Eur. Ceram. Soc*., vol. 21, pp. 2019–2023, 2001, doi: 10.1016/S0955-2219(01)00164-9.

[95] A. Deleniv, S. Abadei, and S. Gevorgian, "Tunable ferroelectric filter-phase shifter", *IEEE MTT-S Int. Microw. Symp. Dig.*, pp. 1267-1270, Apr. 2003, doi: 10.1109/MWSYM.2003.1212600.

[96] F. De Flaviis, N. G. Alexopoulos, and O. M. Stafsudd, "Planar microwave integrated phase-shifter design with high purity ferroelectric material," *IEEE Trans. Microw. Theory Techn.*, vol. 45, no. 6, pp. 963-969, June 1997, doi: 10.1109/22.588610.

[97] A. Kozyrev, V. Osadchiy, A. Pavlov, and L. Sengupta, "Application of ferroelectrics in phase shifter design," in *IEEE MTT-S 2000 Int. Microwave Symp. Dig*., vol. 3, pp. 1355–1358, June 2000, doi: 10.1109/MWSYM.2000.861792.

[98] A. Franc *et al*., "Compact and broadband millimeter-wave electrically tunable phase shifter combining slow-wave effect with liquid crystal technology," *IEEE Trans. Microw. Theory Techn.*, vol. 61, no. 11, pp. 3905-3915, Nov. 2013, doi: 10.1109/TMTT.2013.2282288.

[99] S. Strunck, O. H. Karabey, C. Weickhmann, A. Gaebler, and R. Jakoby, "Continuously tunable phase shifters for phased arrays based on liquid crystal technology," in *Proc. IEEE Int. Symp. Phased Array Syst. Technol*., Oct. 2013, pp. 82–88, doi: 10.1109/ARRAY.2013.6731805.

[100] C. Fritzsch *et al*., "Continuously tunable W-band phase shifter based on liquid crystals and MEMS technology," in *2011 41st European Microwave Conference*, Oct. 2011, pp. 1083-1086, doi: 10.23919/EuMC.2011.6101741.

[101] J. F. Li, H. Xu and D. P. Chu, "Design of liquid crystal based coplanar waveguide tunable phase shifter with no floating electrodes for 60–90 GHz applications," in *Proc. 46th Eur. Microw. Conf. (EuMC)*, pp. 1047–1050, Oct. 2016, doi: 10.1109/EuMC.2016.7824526.

[102] J. H. Dang, R. C. Gough, A. M. Morishita, A. T. Ohta, and W. A. Shiroma, "Liquid-metal-based phase shifter with reconfigurable EBG filling factor," in *Proc. IEEE MTT-S Int. Microw. Symp*., pp. 1-4, May 2015, doi: 10.1109/MWSYM.2015.7167062.

[103] S. Alkaraki, A. L. Borja, J. R. Kelly, R. Mittra, and Y. Gao, "Reconfigurable Liquid Metal-Based SIW Phase Shifter," *IEEE Trans. Microw. Theory Techn.*, vol. 70, no. 1, pp. 323-333, Jan. 2022, doi: 10.1109/TMTT.2021.3124797.

[104] Y. -W. Wu, S. -Y. Tang, J. Churm and Y. Wang, "Liquid metal-based tunable linear phase shifters with low insertion loss, high phase resolution, and low dispersion," *IEEE Trans. Microw. Theory Techn*, doi: 10.1109/TMTT.2023.3248954.

[105] D. M. Hensley, C. G. Christodoulou, and N. Jackson, "A Stretchable Liquid Metal Coaxial Phase Shifter," *IEEE Open Journal of Antennas and Propag.*, vol. 2, pp. 370-374, 2021, doi: 10.1109/OJAP.2021.3063289.

[106] S. J. Mazlouman, X. J. Jiang, A. N. Mahanfar, C. Menon and R. G. Vaughan, "A Reconfigurable Patch Antenna Using Liquid Metal Embedded in a Silicone Substrate," *IEEE Transactions on Antennas and Propagation*, vol. 59, no. 12, pp. 4406-4412, Dec. 2011.

[107] K. Y. Alqurashi and J. R. Kelly, "Continuously tunable frequency reconfigurable liquid metal microstrip patch antenna," 2017 *IEEE International Symposium on Antennas and Propagation & USNC/URSI National Radio Science Meeting*, pp. 909-910, 2017.

[108] Matthew R. Moorefield and Ryan C. Gough and Andy M. Morishita and Jonathan H. Dang and Aaron T. Ohta and Wayne A. Shiroma, "Frequency-tunable patch antenna with liquid-metal-actuated loading slot," *Electronics Letters*, vol. 52, pp. 498-500, March. 2016.

[109] F. Xie, J. J. Adams and M. S. Tong, "An UHF Reconfigurable Liquid-Metal Monopole Antenna Based on a 2-D Surface," *IEEE Transactions on Components, Packaging and Manufacturing Technology*, vol. 11, no. 11, pp. 1980-1987, Nov. 2021.

[110] A. Dey and G. Mumcu, "Microfluidically Controlled Frequency-Tunable Monopole Antenna for High-Power Applications," *IEEE Antennas and Wireless Propagation Letters*, vol. 15, pp. 226-229, 2016.

[111] Morishita A.M., Kitamura C.K.Y., Ohta, A.T., Shiroma, W.A, "Two-octave tunable liquid-metal monopole antenna," *Electronics Letters*, vol. 50, no. 1, pp. 19-20, Jan. 2014.

[112] Shah, Syed I.H., and Sungjoon Lim. 2018. "Microfluidically Frequency-Reconfigurable Quasi-Yagi Dipole Antenna," *Sensors*, vol. 18, no. 9, pp. 2935-2940, Sep. 2018.

[113] Qin, Peng *et al*., "The Design and Manufacturing Process of an Electrolyte-Free Liquid Metal Frequency-Reconfigurable Antenna" *Sensors, vol.* 21, no. 5, pp. 1793, March. 2021.

[114] Arim Ha and Kangwook Kim, "Frequency Tunable liquid metal planar inverted-F antenna", *Electronics Letters*, vol. 52, pp. 100-102, Jan. 2016.

[115] F. Xie and M. S. Tong, "A Novel Reconfigurable Liquid Metal Antenna Controlled by an Impressed Voltage," 2018 *Progress in Electromagnetics Research Symposium (PIERS-Toyama)*, 2018.

[116] J. H Dang, J.H.; Gough, R.C.; Morishita, A.M.; Ohta, A.T.; Shiroma, W.A, "Liquid-metal frequency-reconfigurable slot antenna using air-bubble actuation," Electronics Letters, vol. 51, no. 21, pp. 1630-1632, Oct. 2015.

[117] A. M. Morishita, C. K. Y. Kitamura, A. T. Ohta and W. A. Shiroma, "A Liquid-Metal Monopole Array with Tunable Frequency, Gain, and Beam Steering," *IEEE Antennas and Wireless Propagation Letters*, vol. 12, pp. 1388-1391, 2013.

[118] A. Dey, R. Guldiken and G. Mumcu, "Microfluidically Reconfigured Wideband Frequency-Tunable Liquid-Metal Monopole Antenna," *IEEE Transactions on Antennas and Propagation*, vol. 64, no. 6, pp. 2572-2576, June 2016.

[119] A. Pourghorban Saghati, J. Singh Batra, J. Kameoka and K. Entesari, "A Microfluidically Reconfigurable Dual-Band Slot Antenna with a Frequency Coverage Ratio of 3:1," *IEEE Antennas and Wireless Propagation Letters*, vol. 15, pp. 122-125, 2016.

[120] A. Pourghorban Saghati, J. Singh Batra, J. Kameoka and K. Entesari, "Miniature and Reconfigurable CPW Folded Slot Antennas Employing Liquid-Metal Capacitive Loading," *IEEE Transactions on Antennas and Propagation*, vol. 63, no. 9, pp. 3798-3807, Sept. 2015.

[121] M. Su, X. Geng, Y. Zhang and A. Wang, "Frequency-Reconfigurable Liquid Metal Magnetoelectric Dipole Antenna," *IEEE Antennas and Wireless Propagation Letters*, vol. 20, no. 12, pp. 2481-2485, Dec. 2021

[122] Elley M., Koo, C., McQuilken H., Lawrence B., Li S., Han A., Huff G, "Frequency reconfigurable patch antenna using liquid metal as switching mechanism," *Electronics Letters*, Vol. 49, no. 22, p.p 1370-1371, Oct. 2013.

[123] J. Thews, A. O'Donnell and A. J. Michaels, "Design and analysis of two-dimensional parasitic liquid metal monopole array," *MILCOM 2017 - 2017 IEEE Military Communications Conference (MILCOM)*, pp. 812-816, 2017.

[124] L. Cai and K. Tong, "Fluid Switch for Radiation Pattern Reconfigurable Antenna," *2018 IEEE International Workshop on Electromagnetics: Applications and Student Innovation Competition (iWEM)*, pp. 1-2, 2018.

[125] J. Hao, J. Ren, X. Du, J. H. Mikkelsen, M. Shen and Y. Z. Yin, "Pattern-Reconfigurable Yagi–Uda Antenna Based on Liquid Metal," *IEEE Antennas and Wireless Propagation Letters*, vol. 20, no. 4, pp. 587-591, Apr. 2021.

[126] V. T. Bharambe and J. J. Adams, "Planar 2-D Beam Steering Antenna Using Liquid Metal Parasitics," *IEEE Transactions on Antennas and Propagation*, vol. 68, no. 11, pp. 7320-7327, Nov. 2020.

[127] X. Bai, M. Su, Y. Liu and Y. Wu, "Wideband Pattern-Reconfigurable Cone Antenna Employing Liquid-Metal Reflectors,"*IEEE Antennas and Wireless Propagation Letters*, vol. 17, no. 5, pp. 916-919, May 2018.

[128] S. Alkaraki, J. Kelly and Z. Wang, "Reconfigurable Antenna Using Liquid Metal Vias," 2021 *IEEE International Symposium on Antennas and Propagation and USNC-URSI Radio Science Meeting (APS/URSI)*, 2021, pp. 315-316, doi: 10.1109/APS/URSI47566.2021.9703756

[129] A. A. Gheethan, M. C. Jo, R. Guldiken and G. Mumcu, "Microfluidic Based Ka-Band Beam-Scanning Focal Plane Array," *IEEE Antennas and Wireless Propagation Letters*, vol. 12, pp. 1638-1641, 2013.

[130] A. A. Gheethan, A. Dey and G. Mumcu, "Passive Feed Network Designs for Microfluidic Beam-Scanning Focal Plane Arrays and Their Performance Evaluation," *IEEE Transactions on Antennas and Propagation*, vol. 63, no. 8, pp. 3452-3464, Aug. 2015.

[131] S. Alkaraki, J. Kelly and M. Allayioti, "Radiation Pattern Reconfigurable Antenna Using Liquid Metal Vias," 2021 *IEEE-APS Topical Conference on Antennas and Propagation in Wireless Communications (APWC)*, 2021, pp.1-1, doi: 10.1109/APWC52648.2021.9539582.

[132] J. R. Kelly and M. A. Tanha, "Reconfigurable 26GHz Liquid Metal Antenna Capable of Low Loss Continuous Beam Steering," *2018 IEEE Conference on Antenna Measurements & Applications (CAMA)*, pp. 1-2, 2018.

[133] K. Y. Alqurashi *et al*., "Millimeter Wave Beam Steerable/Reconfigurable Liquid Metal Array Antenna," 2018 *IEEE-APS Topical Conference on Antennas and Propagation in Wireless Communications (APWC)*, 2018.

[134] P. Liu, S. Yang, X. Wang, M. Yang, J. Song and L. Dong, "Directivity-Reconfigurable Wideband Two-Arm Spiral Antenna," *IEEE Antennas and Wireless Propagation Letters*, vol. 16, pp. 66-69, 2017.

[135] A. Ha, M. H. Chae and K. Kim, "Beamwidth Control of an Impulse Radiating Antenna Using a Liquid Metal Reflector," *IEEE Antennas and Wireless Propagation Letters*, vol. 18, no. 4, pp. 571-575, Apr. 2019.

[136] W. Su, S. A. Nauroze, B. Ryan and M. M. Tentzeris, "Novel 3D printed liquid-metal-alloy microfluidics-based zigzag and helical antennas for origami reconfigurable antenna "trees"," 2017 *IEEE MTT-S International Microwave Symposium (IMS)*, pp. 1579-1582, 2017.

[137] Semkin, V., Platonov, O., Kyrö, M. and Räisänen, A.V. "Liquid metal patch antenna and antenna array for WLAN applications," *Microw. Opt. Technol. Lett*., 56: 2462-2464, Jul. 2014.

[138] L. Song, W. Gao and Y. Rahmat-Samii, "3-D Printed Microfluidics Channelizing Liquid Metal for Multipolarization Reconfigurable Extended E-Shaped Patch Antenna," *IEEE Transactions on Antennas and Propagation*, vol. 68, no. 10, pp. 6867-6878, Oct. 2020.

[139] Z. Chen, H. Wong and J. Kelly, "A Polarization-Reconfigurable Glass Dielectric Resonator Antenna Using Liquid Metal," *IEEE Transactions on Antennas and Propagation*, vol. 67, no. 5, pp. 3427-3432, May 2019.

[140] C. Xu, Z. Wang, Y. Wang, P. Wang and S. Gao, "A Polarization-Reconfigurable Wideband High-Gain Antenna Using Liquid Metal Tuning," *IEEE Transactions on Antennas and Propagation*, vol. 68, no. 8, pp. 5835-5841, Aug. 2020

[141] Xu, C, Wang, Y, Wu, J, Wang, Z," Parasitic circular patch antenna with continuously tunable linear polarization using liquid metal alloy,"

Microwave Optical Technology Letter, vol. 61, no.3, pp. 727– 733, Mar. 2019.

[142] C. Wang, J. C. Yeo, H. Chu, C. T. Lim and Y. -X. Guo, "Design of a Reconfigurable Patch Antenna Using the Movement of Liquid Metal," *IEEE Antennas and Wireless Propagation Letters*, vol. 17, no. 6, pp. 974-977, June 2018.

[143] Lee, M, Son, H, Lim, D, Lee, S, Lim, S, "Liquid-metal-fluidically polarization reconfigurable microstrip patch antenna," *Microwave Optical Technology Letter*, vol. 61, pp. 2306– 2314, Oct. 2019.

[144] M. R. Moorefield, A. T. Ohta and W. A. Shiroma, "A Polarization-Reconfigurable Antipodal Dipole Antenna Using Liquid Metal," 2018 *Asia-Pacific Microwave Conference (APMC)*, pp. 1250-1252, 2018.

[145] Zhe Chen, H. Wong, Jun Xiang and Bin-Long Bu, "A polarization-reconfigurable liquid dielectric resonator antenna with 3D printing fabrication," 2017 *International Workshop on Electromagnetics: Applications and Student Innovation Competition*, pp. 121-123, 2017.

[146] C. Wang, Y. Guo, J. C. Yeo and C. T. Lim, "Improving the Radiation Efficiency of Liquid Metal Antenna with Polarization Agility," 2018 *IEEE International Symposium on Antennas and Propagation & USNC/URSI National Radio Science Meeting*, pp. 941-942, 2018.

[147] M. Champion, D. Jackson, B. Cumby and E. Belovich, "Polarization Reconfigurable Antennas Using a Liquid Metal Switching Mechanism," 2017 *IEEE International Symposium on Antennas and Propagation & USNC/URSI National Radio Science Meeting*, pp. 415-416, 2017.

[148] Sarabia K.J., Ohta A.T., Shiroma W.A, "Pixelated dual-dipole antenna using electrically actuated liquid metal", *Electronics Letters*, vol. 55, no.19, pp. 1032-1034, Sep. 2019.

[149] M. Wang, M. R. Khan, M. D. Dickey and J. J. Adams, "A Compound Frequency- and Polarization- Reconfigurable Crossed Dipole Using Multidirectional Spreading of Liquid Metal," *IEEE Antennas and Wireless Propagation Letters*, vol. 16, pp. 79-82, 2017.

[150] Y. Liu, Q. Wang, Y. Jia and P. Zhu, "A Frequency- and Polarization-Reconfigurable Slot Antenna Using Liquid Metal," *IEEE Transactions on Antennas and Propagation*, vol. 68, no. 11, pp. 7630-7635, Nov. 2020.

[151] L. Li, X. Yan, H. C. Zhang and Q. Wang, "Polarization-and Frequency-Reconfigurable Patch Antenna Using Gravity-Controlled Liquid Metal," *IEEE Transactions on Circuits and Systems II: Express Briefs*, doi: 10.1109/TCSII.2021.3119040.

[152] S. Yee, D. Weinstein, J. Fiering, D. White and A. Duwel, "A miniature reconfigurable circularly polarized antenna using liquid microswitches," 2015 *IEEE* 16*th Annual Wireless and Microwave Technology Conference (WAMICON)*, pp. 1-5, 2015.

[153] J. Thews, A. O'Donnell and A. J. Michaels, "Design and analysis of dual helix liquid metal antenna," *MILCOM* 2017 - 2017 *IEEE Military Communications Conference (MILCOM)*, 2017.

[154] K. S. Elassy, M. A. Rahman, W. A. Shiroma and A. T. Ohta, "Liquid-Metal Nodal Sheet for Reconfigurable Devices and Circuits," *IEEE Access*, vol. 8, pp. 167596-167603, 2020.

[155] Deng, Guangsheng, Fang, Linying, Yang, Jun, Yin, Zhiping and Fang, Yong. "Liquid metal-based metamaterial with high-temperature sensitivity: Design and computational study," *Open Physics*, vol. 19, no. 1, pp. 735-741, Nov. 2021.

[156] J. Xu, Y. Fan, R. Yang, Q. Fu, and F. Zhang, "Realization of switchable EIT metamaterial by exploiting fluidity of liquid metal," Opt. Express, vol. 27, no.3, pp. 2837-2843, 2019.

[157] Z. Lei et al., "A flexible metamaterial based on liquid metal patterns embedded in magnetic medium for lightweight microwave absorber," Materials Research Bulletin, Vol. 137, no. 111199, May. 2021.

[158] Xing-Liang Tian, Cai-Xing Hu, Dan Zhang, Hai-Feng Zhang, "A gravity field tailored metamaterial absorber containing liquid metal for polarization separation," Physics B: Condensed Matter, Vol. 614, no. 413030, Aug. 2021.

[159] Liang, Q., Yang, Z., Guo, J. *et al.* "A high-efficient tunable liquid metal-based electromagnetic absorbing metamaterial," *J Mater Sci: Mater Electron*, Vol. 31, pp. 19242–19247, Sep. 2020.

[160] D. Lim and S. Lim, "Liquid-Metal-Fluidically Switchable Metasurface for Broadband and Polarization-Insensitive Absorption," *IEEE Access*, vol. 6, pp. 40854-40859, 2018.

[161] Ling K, Kim HK, Yoo M, Lim S. "Frequency-Switchable Metamaterial Absorber Injecting Eutectic Gallium-Indium (EGaIn) Liquid Metal Alloy," *Sensors*, vol.11, no. 11, pp. 28154-28165, 2015.

[162] Ling K, Kim K, Lim S. "Flexible liquid metal-filled metamaterial absorber on polydimethylsiloxane (PDMS)," Opt Express, Vol. 16, No. 23, Aug. 2015

[163] H. Kim, D. Lee, and S. Lim, "Wideband-Switchable Metamaterial Absorber Using Injected Liquid Metal," *Sci Rep*, Vol. 6, pp. 31823, Aug. 2016.

[164] Z. H. Nick, C. E. Tabor, R. L. Harne, "Liquid metal microchannels as digital sensors in mechanical metamaterials," Extreme Mechanics Letters, Vol. 40, no. 100871, Oct. 2020.

[165] Ren Y, Duan M, Guo R, Liu J. "Printed Transformable Liquid-Metal Metamaterials and Their Application in Biomedical Sensing," *Sensors*, vol. 19, no.21, pp. 6329, 2021.

[166] Patel, SK, Kosta, Y. "Liquid metamaterial based microstrip antenna," Microw. Opt. Technol. Lett.; Vol. 60, pp. 318-322, Jan. 2018.

[167] Y. Liu, Z. Liu, Q. Wang and Y. Jia, "Low-RCS antenna array with switchable scattering patterns employing microfluidic liquid metal alloy-based metasurface," *IEEE Transactions on Antennas and Propagation*, vol. 69, no. 12, pp. 8955-8960, Dec. 2021.

[168] L. Chen, Y. Ruan, H. Yang Cui, "Liquid metal metasurface for flexible beam-steering," Opt. Express, vol. 27, no. 16, pp. 23282-23292, 2019.

[169] Qian T. "Reconfigurable Metasurface Antenna Based on the Liquid Metal for Flexible Scattering Fields Manipulation," *Micromachines*. Vol.3, No. 12, Feb. 2021.

[170] S. Ghosh and S. Lim, "A Multifunctional Reconfigurable Frequency-Selective Surface Using Liquid-Metal Alloy," *IEEE Transactions on Antennas and Propagation*, vol. 66, no. 9, pp. 4953-4957, Sept. 2018.

[171] J. Wang, S. Liu, S. Guruswamy, A. Nahata, "Reconfigurable terahertz metamaterial device with pressure memory," Opt. Express, vol. 22, no.4, pp. 4065-4074, 2014.

[172] K. Yamagishi, W. Zhou, T. Ching, S. Y. Huang, M. Hashimoto, "Ultra-Deformable and Tissue-Adhesive Liquid Metal Antennas with High Wireless Powering Efficiency," *Advanced Material*, vol. 33, no. 2008062, 2021.

[173] D. L. Diedhiou, O. de Sagazan, R. Sauleau and A. V. Boriskin, "Contactless Microstrip Transition for Flexible Microfluidic Circuits and Antennas," *IEEE Antennas and Wireless Propagation Letters*, vol. 14, pp. 1502-1505, 2015.

[174] M. N. Ramli *et al*., "Flexible dual-band AMC-backed PDMS antenna with fluidic metal for WBAN and WLAN," *12th European Conference on Antennas and Propagation (EuCAP 2018)*, pp. 1-3, 2018.

[175] S. Dobir Hossain, A. Arif, B. Lohani and R. C. Roberts, "Flexible EGaIn Liquid Metal Microstrip Patch Antenna Based Pressure Sensor," *2021 IEEE Sensors*, pp. 1-4, 2021.

[176] G. J. Hayes, J. So, A. Qusba, M. D. Dickey and G. Lazzi, "Flexible Liquid Metal Alloy (EGaIn) Microstrip Patch Antenna," *IEEE Transactions on Antennas and Propagation*, vol. 60, no. 5, pp. 2151-2156, May 2012.

[177] W. Meng, L. Zhifu, D. Jian, "Liquid Metal-Embedded Layered-PDMS Antenna for Flexible and Conformal Applications," *Frontiers in Physics*, vol. 10, 2022.

[178] M. Cosker, L. Lizzi, F. Ferrero, R. Staraj and J. Ribero, "Realization of 3-D Flexible Antennas Using Liquid Metal and Additive Printing Technologies," *IEEE Antennas and Wireless Propagation Letters*, vol. 16, pp. 971-974, 2017.

[179] Zhu J, Cheng H. "Recent Development of Flexible and Stretchable Antennas for Bio-Integrated Electronics," *Sensors*. Vol. 12, no.18, pp. 4364, 2018.

[180] J. Zhou, J. Dong, M. Wang and H. Luo, "A 3D printed dual-band antenna using liquid metal for wearable bracelets communications," *2020 IEEE MTT-S International Wireless Symposium (IWS)*, pp. 1-3, 2020.

[181] Y. Huang, Y.Wang, L. Xiao, H. Liu, W. Dong and Z. Yin, "Robust, multiscale liquid-metal patterning enabled by a sacrificial sealing layer for flexible and wearable wireless powering" , Lab on Chip, no. 21, Jul. 2014.

[182] A. Vorobyov, C. Henemann and P. Dallemagne, "Liquid Metal based antenna for wearable electronic," *2016 10th European Conference on Antennas and Propagation (EuCAP)*, pp. 1-3, 2016.

[183] B. Yao et al, "Highly stretchable and mechanically tunable antennas based on three dimensional liquid metal network," *Materials Letters*, vol. 270, no. 127727, Jul. 2020.

[184] Y. Jeong *et al*., "A skin-attachable, stretchable integrated system based on liquid GaInSn for wireless human motion monitoring with multi-site sensing capabilities," *NPG Asia Mater* vol. **9,** no. 443, 2017.

[185] S. Cheng, Z. Wu, P. Hallbjorner, K. Hjort and A. Rydberg, "Foldable and Stretchable Liquid Metal Planar Inverted Cone Antenna," *IEEE Transactions on Antennas and Propagation*, vol. 57, no. 12, pp. 3765-3771, Dec. 2009.

[186] Meng Wang, Ian M. Kilgore, Michael B. Steer, Jacob J. Adams, "Characterization of Intermodulation Distortion in Reconfigurable Liquid

Metal Antennas," *IEEE Antennas and Wireless Propagation Letters*, Vol. 17, No. 2, 2018.

[187] R. Xue *et al*., "Pumping of ionic liquids by liquid metal ‐ enabled electrocapillary flow under DC ‐ biased AC forcing," *Advanced Materials Interfaces*, vol. 7, no .14, 2020, doi: org/10.1002/admi.202000345.